Omidvar Hamidreza (Orcid ID: 0000-0001-8124-7264)

Song Jiyun (Orcid ID: 0000-0002-9483-0501)

Wang Zhihua (Orcid ID: 0000-0001-9155-8605)

Bou-Zeid Elie (Orcid ID: 0000-0002-6137-8109)

Rapid Modification of Urban Land Surface Temperature during Rainfall

Hamidreza Omidvar[1], Jiyun Song[2], Jiachuan Yang[1], Gilad Arwatz[2], Zhi-Hua Wang[2], Marcus Hultmark[3], Kamil Kaloush[2], Elie Bou-Zeid[1*]

[1]Department of Civil and Environmental Engineering, Princeton University, Princeton, NJ, USA.

[2]School of Sustainable Engineering and the Built Environment, Arizona State University, Tempe, AZ, USA.

[3]Department of Mechanical and Aerospace Engineering, Princeton University, Princeton, NJ, USA.

[*]Corresponding author: Elie Bou-Zeid (ebouzeid@princeton.edu)

Key points:

This is the author manuscript accepted for publication and has undergone full peer review but has not been through the copyediting, typesetting, pagination and proofreading process, which may lead to differences between this version and the Version of Record. Please cite this article as doi: 10.1029/2017WR022241

- A model is developed for urban pavement and runoff temperature during rainfall, and validated against experimental data.
- Application over a parking lot indicates faster cooling of pervious surfaces, compared to impervious, due to infiltration.
- During rainfall, heat transfer is dominated by terms associated with water flux and subsurface heat extraction.

Abstract

This paper examines runoff dynamics and heat transfer during rainfall over urban surfaces, in particular pavements. A kinematic wave approach is combined with heat storage and transfer schemes to develop a model for pervious and impervious pavements. The resulting framework is a numerical prognostic model that can simulate the temperature fields in the subsurface and runoff layers to capture the rapid cooling of the surface, as well as the thermal pollution advected in the runoff. Extensive field measurements are conducted over several types of experimental pavements in Arizona to probe the physics and then to validate the model. The experimental data and the model results are in good agreement, and their joint analysis elucidates the physics of the rapid heat transfer from the subsurface to the runoff. A demonstrative application of the model over a (hypothetical) parking lot, with impervious or pervious asphalt, is then presented. It illustrates that the rate of ground surface temperature cooling for the impervious pavement is lower than the pervious one (where infiltration is very effective at removing heat). Finally, the analysis of the energy budgets unravels the relative importance of the various physical mechanisms in transferring heat from the subsurface to the runoff and the atmosphere. This transfer is dominated by terms associated with water flux and subsurface heat extraction, while latent, sensible, and radiative heat fluxes are minor contributors. The findings underline the importance of including rainfall-induced cooling in geophysical models that seek to study urban heat islands or urban precipitation modification.

Keywords: pavements, urban heat island, precipitation, thermal pollution, surface energy budget

1 Introduction

Land surface temperature is a critically important parameter that exerts a strong influence on many earth systems characteristics such as the partitioning of surface energy budgets and the static stability and turbulence intensity in the atmospheric boundary layer (ABL) (de Arellano et al., 2015; Stull, 1988). It also modulates a wide range of processes and phenomena of significant practical interest such as ecosystem function, evaporation, and irrigation demand (Brutsaert, 2005; Shuttleworth, 2012), as well as secondary circulations such as sea breezes (de Arellano et al., 2015; Stull, 1988). Urbanization, which is proceeding at an unprecedented rate in human history with estimates of a doubling of urban land use by 2050 compared to 2015 (Angel, 2012; Grimmond, 2007), strongly alters the land surface temperature. This alteration is almost invariably an increase due to a range of modifications to the surface texture and properties including reduced albedo, reduced moisture retention, and increased thermal effusivity (Bounoua et al., 2015; Oke, 1973, 1982; Ramamurthy et al., 2014). This widely observed phenomenon is known as the urban heat island (UHI) effect. While the surface and atmospheric manifestations of the UHI have been widely studied, the thermal effect of urbanization also extends to the subsurface and the so-called subUHI is now increasingly being investigated (Ferguson & Woodbury, 2007; Phelan et al., 2015; Zhan et al., 2014).

Given these UHI thermal anomalies that extend from the subsurface to the atmosphere, it is natural to expect a concomitant impact on the temperature of surface water bodies resulting from hotter urban runoff, and yet this impact has received little attention so far. Since the rain temperature is expected to be lower than the urban surface temperature, the fast initiation of runoff on impervious urban surfaces (e.g. paved roads and parking lots, sidewalks or brick surfaces, rooftops) rapidly extracts and advects the heat stored in these pavements. When this runoff eventually merges with the streams (directly or after being conveyed in drainage systems), it induces intensive thermal pollution that can severely impact stream ecology and health (Krause et al., 2004; Nelson & Palmer, 2007). Concurrently, as runoff extracts and advects heat, it cools down these urban surfaces very quickly (Ramamurthy & Bou-Zeid, 2014). This abrupt cooling of the surface induces a rapid change in atmospheric stability and dynamics, and can potentially influence the subsequent development of rain-generating storms. Nevertheless, current models where such cooling would have a significant impact (such as the Weather Research and Forecasting - WRF - model) do not account for it. Hence, understanding the processes controlling heat transfer from hot surfaces, how the surface and runoff temperatures evolve during a rainfall event, and how to build prognostic models for this evolution would help us develop a deeper understanding of a wide range of environmental phenomena and improve the prediction skills of various geophysical models. These goals frame the aims of this paper.

The mechanisms of heat transfer from paved surfaces during rainfall remain poorly understood due to the difficulties in capturing the many important physical processes and

parameters in experiments and models. Van Buren et al. (2000) proposed a heat transfer model that includes all surface energy budgets to compute the ground surface temperature during the rainfall; however, their study did not have a model for runoff dynamics (here, runoff dynamics refer to the runoff depth and velocities that reflect mass and momentum conservation) and estimated the runoff temperature based on the rainfall and surface temperature of the pavement (a similar approach was adopted in Cohard et al., (2017)). Janke et al. (2009) suggested a more complete model solving a one-dimensional (1D) runoff model numerically coupled with a 1D heat budget for both the subsurface and the runoff. In another study by the same authors (Herb et al., 2009), an analytical model for the runoff dynamics was derived and coupled with a heat transfer model to estimate the surface and runoff temperatures. However, in both studies, the runoff was assumed to be in the thermal equilibrium with the surface all the time (no vertical temperature gradient was assumed in the runoff) and no infiltration was allowed. Kertesz and Sansalone (2014) used field measurements conducted on asphalt pavements in conjunction with a heat balance model that combines the models used in the previous studies (Herb et al., 2009; Janke et al., 2009; Kim et al., 2008; Sansalone & Teng, 2005; Thompson et al., 2008; Van Buren et al., 2000) to study the thermal energy transfer of rainfall storms; however, this study again did not consider runoff dynamics. In addition, the field measurements in these previous studies did not include some crucial thermal parameters such as radiation components or resolved temperature gradients in the runoff layer.

Although some of the assumptions used in the previous studies (such as vertical thermal equilibrium) might seem reasonable for the problem, they might breakdown during the early-time evolution and for spatial evolution over short pavements. Therefore, such assumptions cannot be treated as *a priori* knowledge without validation. In addition, the lack of accurate measurements of the important input and output variables thus far prevented direct evaluation of these assumptions, or the development of more complete models to test their validity. Finally, the increasingly-important cooling down of pervious pavements by infiltration (or a combination of infiltration and runoff) remains unstudied, despite the broadening applications of such pavements as urban heat island mitigation measures. These remaining challenges and open questions frame the design of the experimental and modeling components of the present study.

The main objective here is hence to bridge the gaps in the observation and modeling of heat transfer from urban pavements during rainfall. We develop a complete model for heat transfer for both impervious and pervious pavements, accounting for all the physical processes in the problem (model physics in section 2 and numerics in section 3). We then conduct a set of field measurements using novel sensors and collect data over pavements with different thermal properties (section 4) in order to probe the physics that we are parameterizing in the model and to then validate the model (section 5). We finally do a demonstrative application of the model over a hypothetical parking lot (section 6) where we compare pervious and impervious pavements. The paper ends with a discussion of model limitations (section 7), and a conclusion and outlook (section 8).

2 Model description

Most human-made urban pavements have very low permeability, and the infiltration can be safely neglected. Given the propensity of these pavements to cause urban flooding and to heat up significantly, another class of engineered pavements being developed in cities are ones with very high permeability, such that no runoff initiates and infiltration and evaporation play the key role in flood mitigation and surface cooling. Hence, in this study, we focus on studying the heat and water transfer processes when (i) the pavement is fully impervious and has a non-zero slope such that the runoff initiates (and needs to be modeled) as the rain starts and the amount of infiltration is negligible, or (ii) the pavement is fully pervious with no runoff formation during the rainfall since all the water infiltrates into the unsaturated ground. For both cases, all heat transfer mechanisms and the energy budgets of the ground surface, as well that of the top surface of the runoff layer for impervious pavements, are represented and modeled. Natural surfaces and vegetated urban surfaces fall in between these two permeability limits. While we have not conducted experiments on such intermediate surfaces since they are not the focus of the present study, the thermal budget model we propose can in fact be applied to a mixture of both runoff and infiltration for various surfaces with different permeabilities if the saturation level of the top soil layer is correctly tracked and infiltration into unsaturated and then saturated ground is correctly modeled.

2.1 Fully impervious pavements

A comprehensive model to predict the surface and runoff temperatures must take into account the runoff dynamics (introduced here in section 2.1.1), as well as the thermal energy budget and various heat transfer models between the runoff, the pavement, and the air (presented below in 2.1.2).

2.1.1 Runoff dynamics

The runoff on impervious pavements is modeled as a two-dimensional (2D, streamwise and vertical) unsteady overland flow. The vertically-averaged mass conservation (continuity) equation for such flow is written as (Brutsaert, 2005)

$$\frac{\partial h(x,t)}{\partial t}+\frac{\partial q(x,t)}{\partial x}=S(x,t), \tag{1}$$

where x is the distance from the point where the runoff starts (m); t is the time (s); $h(x,t)$ is the full depth of the flow (m); $q(x,t)$ is the flow rate per unit cross-stream width ($m^2\ s^{-1}$); and $S(x,t)$ is a source/sink term ($m\ s^{-1}$). For an impervious surface where infiltration is negligible, the only source term is the rainfall since the contribution of evaporation during rainfall to the sink term is negligible in comparison. Note that the evaporation role is not negligible in the heat budget of the problem as will be discussed in section 2.1.2. Therefore, $S(x,t)=i(x,t)$, where i is the rainfall intensity ($m\ s^{-1}$).

The flow rate and bulk (average) velocity $U(x,t)$ can be expressed in terms of the flow depth as

$$q(x,t) = U(x,t)h(x,t) \qquad ; \qquad U(x,t) = \frac{1}{h}\int_0^h u(x,y,t)\,dy. \tag{2}$$

In this equation, $u(x,y,t)$ is the spatially-local streamwise velocity (m s^{-1}), and y is the vertical coordinate (m).

In addition to the mass conservation equation, a momentum budget for the flow is needed. The kinematic wave approach for shallow water is used here; it assumes that the friction force in the horizontal direction is in balance with the gravity force in the same direction. It can be formulated for a laminar flow and a hydrodynamically smooth surface (where the viscous drag dominates over surface form drag) as follows

$$\nu\frac{\partial^2 u(x,y,t)}{\partial y^2} = -g\sin(\theta) \approx -g\theta = -gs_0, \tag{3}$$

where ν is the runoff kinematic molecular viscosity; g = 9.81 m s^{-2} is the gravitational acceleration; θ (rad) is the angle of the pavement surface relative to the horizontal axis; and s_0 is the pavement slope, which is equal to θ for small values. Upon integrating equation (3) from y=0 to y=h, with a no-slip boundary condition at y=0, and zero shear stress at y=h (the interface between the runoff and the air), the following equation for the horizontal velocity profile is obtained

$$u(x,y,t) = \frac{gs_0}{\nu}\left(hy - y^2/2\right). \tag{4}$$

For a rough surface (where the form drag over roughness elements is no longer negligible), since the flow remains laminar under most conditions as we will discuss later, if one considers that a

stagnant water layer is "trapped" in the roughness sublayer, equation (4) can also be applied assuming again a no-slip boundary condition, but this condition should be imposed at the crest of the roughness elements and *y* should be considered as the height above that crest. A finite slip boundary condition (or equivalently a no-slip at some depth below the crest) would be more accurate since as the runoff starts, the trapped water layer might generate circulations inside the roughness layer that produce a finite non-zero velocity, but if the flow depth is much larger than the roughness and most of the flow occurs above this roughness, the results with zero and non-zero slip would be indistinguishable as the finite slip boundary condition just adds a small constant to equation (4). Thus, we will not be concerned with generalizing equation (4) in the current study and will use it for both smooth and rough surfaces as long as the flow is laminar (validation shown later justifies this assumption). Using equation (4), the runoff bulk velocity can be computed from its definition in equation (2):

$$U(x,t)=\frac{gs_0h^2}{3\nu}. \tag{5}$$

The system of equations (1), (2), and (5) can be solved for $h(x,t)$ numerically for arbitrary initial and boundary conditions (or for non-constant and non-uniform rainfall intensities); however, if we assume $h(0,t)=0$ as the boundary condition, and a dry pavement surface $h(x,0)=0$ as the initial condition, with a constant and uniform rainfall intensity, we can obtain the following analytical solution for $h(x,t)$ using the method of characteristics (Parlange, Rose, Sander, Campbell, & Barry, 1983):

$$h(x,t)=\begin{cases} it & \text{for } x \geq \dfrac{t^3 s_0 g i^2}{3\nu} \quad \text{homogeneous unsteady} \\ \left(\dfrac{3x\nu i}{s_0 g}\right)^{\frac{1}{3}} & \text{for } x < \dfrac{t^3 s_0 g i^2}{3\nu} \quad \text{inhomogeneous steady} \end{cases} . \qquad (6)$$

Equation (6) shows that the runoff depth solution has two parts: (1) one where the depth is unsteady in time but homogeneous along *x,* and (2) another where runoff depth does not change with *t* (steady) but varies in *x* (inhomogeneous).

Combining equations (4), (6) and the continuity equation ($\partial u/\partial x+\partial v/\partial y=0$), and imposing the boundary condition of v=0 at y=0, yields the following vertical velocity profile

$$v(x,y)=\begin{cases} 0 & \text{for } x \geq \dfrac{t^3 s_0 g i^2}{3\nu} \quad \text{homogeneous unsteady} \\ -\dfrac{s_0 g h y^2}{6\nu x} & \text{for } 0 < x < \dfrac{t^3 s_0 g i^2}{3\nu} \quad \text{inhomogeneous steady} \end{cases} . \qquad (7)$$

According to equation (7), the vertical velocity is non-zero in the steady part of the flow, and zero in the unsteady part. For the unsteady part, this physically implies that the rainfall contributes by building up the rainfall depth instead of penetrating into existing runoff and generating a vertical flow.

2.1.2 Runoff-pavement heat transfer

Figure 1a shows all the important thermal exchange processes that need to be considered in the modeling framework to predict the surface and runoff temperatures for an impervious

surface. In the runoff, the horizontal diffusion can be safely assumed to be much smaller than the advection term in the same direction; however, the vertical velocity we derived in equation (7) is much smaller than the horizontal velocity, and its effect is likely to be comparable with or even smaller than the vertical diffusion. Therefore, in the vertical direction, we consider both the thermal diffusion and advection components of the heat budget. Hence, the transient heat budget equation for the runoff is given by

$$\frac{\partial T_w(x,y,t)}{\partial t} = D_w \frac{\partial^2 T_w(x,y,t)}{\partial y^2} - \left(u \frac{\partial T_w(x,y,t)}{\partial x} + v \frac{\partial T_w(x,y,t)}{\partial y} \right), \tag{8}$$

where $T_w(x,y,t)$ is the runoff water temperature (ºC) and D_w is the thermal diffusivity of the runoff water ($m^2\ s^{-1}$) (this thermal diffusivity is not necessary the molecular diffusivity because of the additional mixing due to rain drops or turbulence, as we will discuss later in this section). 2D heat conduction can be assumed in the subsurface obeying

$$\frac{\partial T_g(x,y,t)}{\partial t} = D_g \left(\frac{\partial^2 T_g(x,y,t)}{\partial y^2} + \frac{\partial^2 T_g(x,y,t)}{\partial x^2} \right), \tag{9}$$

where $T_g(x,y,t)$ is the subsurface temperature (ºC), and $D_g = k_g \rho_g^{-1} c_g^{-1}$ is the thermal diffusivity of the subsurface ($m^2\ s^{-1}$) where k_g, ρ_g, and c_g are the thermal conductivity ($W\ m^{-1}\ K^{-1}$), density ($kg\ m^{-3}$) and specific heat ($J\ kg^{-1}\ K^{-1}$), respectively. Figure 1b shows the runoff and the subsurface domains for which coupled equations (8) and (9) should be solved, along with the surface energy budgets of the boundaries. A numerical solution is needed for general boundary and initial conditions.

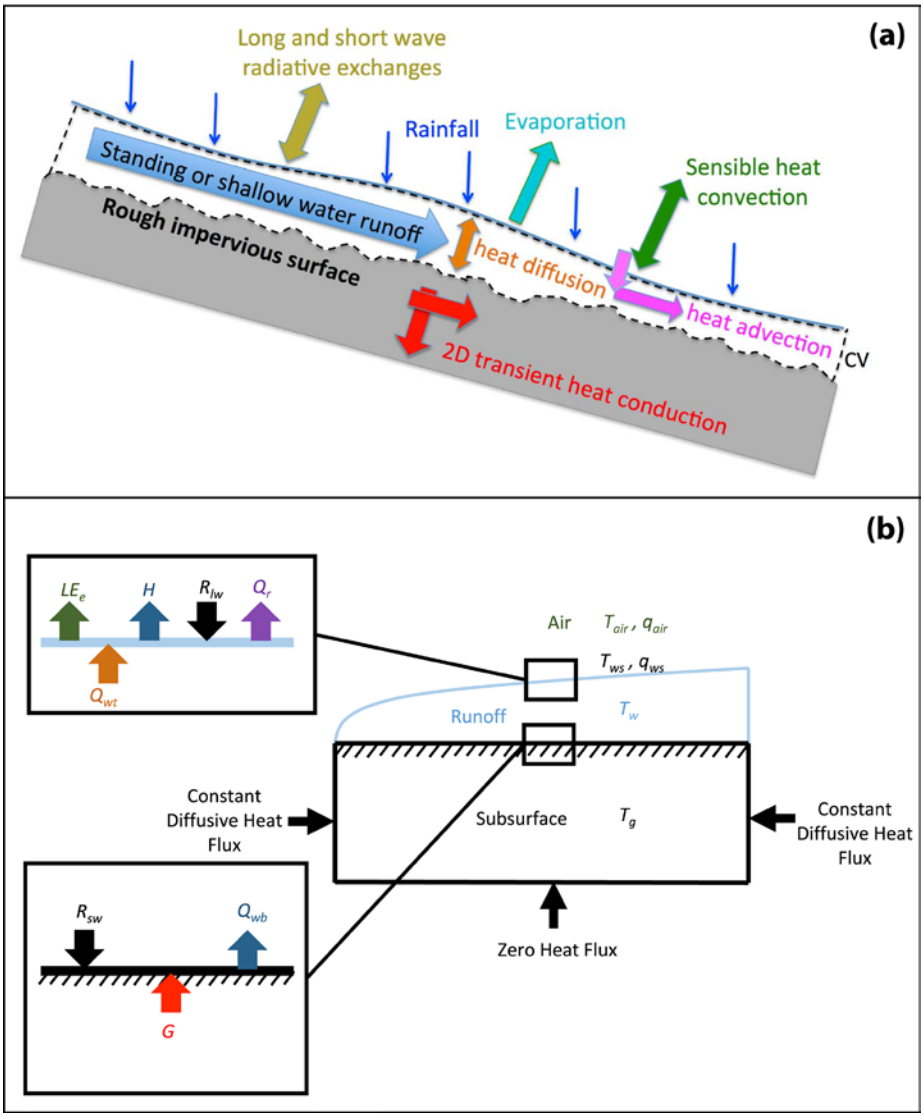

Figure 1. (a): Important thermal processes in the heat budget of the problem illustrated for a rough surface, (b): Runoff and subsurface domains and their boundary conditions. The variables are as defined in section 2.1.2.

The required thickness of the subsurface domain (h_g) is calculated to ensure an adiabatic lower boundary condition. The depth to which the heat penetrates into the subsurface is

proportional to the heat diffusion length scale L_{diff} in the subsurface, and the domain should extend to several times that length scale to guarantee that the bottom boundary condition has no impact on the solution of the heat budget equations. Hence, h_g is given by

$$h_g = \alpha L_{diff} = \alpha \sqrt{D_g t_{total}}, \tag{10}$$

where t_{total} is the total time for which the heat equations are integrated (s). α is a proportionality constant that should be large enough to ensure insensitivity to bottom boundary conditions of the subsurface domain. Based on the sensitivity tests we conducted, a value of $\alpha = 5$ is found to satisfy this criterion (see the supporting information section S4 for the results).

Pavement surface water holding capacity

Because of pavement roughness or hydrophilic properties, the runoff does not begin as soon as the rain starts on the impervious pavements. First, a very thin layer of stationary water accumulates; then the runoff starts above it. To take this into account in the model, we consider that a stagnant layer of water first develops after rain initiation, and then subsequently runoff begins. The total thickness (δ) of this layer depends on the pavement roughness, and it can be measured for different impervious pavements (see section 4). This stagnant layer remains stationary during the entire rainfall event (in agreement with the zero slip boundary condition at the top of that layer discussed in section 2.1.1) and the runoff layer effectively starts at the top of the stagnant layer. The heat equation solved in the stagnant layer is similar to the one for the runoff in equation (8), except that the advection term is zero because we are assuming that the horizontal and vertical velocities there are negligible. The bottom of this layer is the interface

between the water and the ground. The time t_δ required to form this stagnant water layer is a function of its depth δ and of the rain intensity (i):

$$t_\delta = \frac{\delta}{i}. \tag{11}$$

Mixing due to the rain drops

Although the runoff Reynolds number is within the range suggesting laminar flow in all present experiments and simulations (see Supporting Information section S6), the mixing due to falling rain drops impact on, and penetration into, the runoff layer is not negligible. We take into account this effect by assuming that the runoff thermal diffusivity (D_w) in equation (8) is an effective thermal diffusivity (D_{eff}) instead of the molecular thermal diffusivity (D_{mol}):

$$D_w = D_{eff} = \beta D_{mol}, \tag{12}$$

where β >1 but its exact value will be estimated as a calibration parameter for the runoff-impervious pavements model. β is dependent on the rainfall intensity; it is thus a constant for constant rainfall intensity. More general models for this parameter could be developed.

Boundary conditions

Figure 1b shows the thermal boundary conditions used. For the effluent boundary of the water layer (right boundary in figure), no boundary condition is needed for the heat equation because an upwind scheme is used for the discretization of the horizontal advection term in equation (8), and the last point at the downstream can be calculated without specifying a boundary condition.

The top boundary of the runoff is the interface between the air and the water. A surface energy budget equation is solved for this boundary at each time step of the simulation as follows:

$$R_{lw} + LE_e + Q_r + H + Q_{wt} = 0, \tag{13}$$

where the terms represent the energy fluxes respectively associated with the net longwave radiation, evaporation, rainfall on the surface, heat exchange between the water surface and the air, and heat exchange between water surface and the runoff (due to conduction and rainfall mixing), all expressed in (W m^{-2}). All terms are defined and written as positive into the surface (gain) and negative out of the surface (loss); this is not the conventional approach for writing the surface energy budget but is more consistent in the current model where more terms are involved. Note that liquid water for the purposes of this study can be considered opaque to longwave radiation, and completely transparent to shortwave radiation (Hale & Querry, 1973; Vercauteren et al., 2011). Therefore, the longwave radiation term appears only at the top boundary, and the shortwave radiation should be considered for the ground surface energy budget. R_{lw}, Q_r, and Q_{wt} are given by:

$$R_{lw} = LW_{down} - LW_{up} \tag{14}$$

$$LW_{up} = \left(1-\varepsilon\right) LW_{down} + \varepsilon\sigma T_{ws}^{\ 4} \tag{15}$$

$$Q_{wt} = -k_w \left(\frac{\partial T_w}{\partial y} \right)_{y=h} \tag{16}$$

$$Q_r = i\rho_w c_w \left(T_r - T_{ws}\right), \tag{17}$$

where LW_{down} is the downwelling longwave radiation (W m^{-2}) and is an input to the model from the measurement data (if not measured this term can be modeled using approaches derived from the Brutsaert (1975) model); LW_{up} is the upwelling longwave radiation (W m^{-2}) computed as an output, ε and σ are the water surface emissivity and Stefan-Boltzmann constant, respectively; $k_w = \rho_w c_w D_w$ is the effective water thermal conductivity (W m^{-1} K^{-1}); ρ_w is water density (kg m^{-3}); c_w is the water specific heat capacity (J kg^{-1} K^{-1}); T_{ws} is the water surface temperature; and T_r is the rain temperature.

The latent and sensible heat fluxes between the water surface and the air are modeled using bulk formulas (Brutsaert, 2005):

$$H = C_H \rho_{air} c_{air} u_{air} (T_{air} - T_{ws}), \tag{18}$$

$$LE_e = C_E L_e \rho_{air} u_{air} (q_{air} - q_{ws}), \tag{19}$$

where C_H is the heat transfer coefficient; C_E is the water vapor transfer coefficient; ρ_{air} is the air density (kg m^{-3}); c_{air} is its heat capacity (J kg^{-1} K^{-1}). u_{air} is the wind speed (m s^{-1}), T_{air} the temperature, and q_{air} the specific humidity of air measured at some height z_m above the water surface; L_e is the latent heat of evaporation of water (kJ kg^{-1}). The air right above the water surface is almost fully saturated, and the air specific humidity at this point, q_{ws}, can be estimated as the saturation specific humidity. Following the Clausius-Clapeyron relation, this saturation q_{ws} is a function of the water surface temperature $q_{ws=}$ $q^*(T_{ws})$, where the asterisk (*) superscript indicates the saturation condition. q^* is calculated using a polynomial approximation function (Lowe, 1977).

C_H and C_E are computed using the Monin-Obukhov similarity theory (Monin & Obukhov, 1954). If we assume neutral stability (a reasonable assumption since we are very close to the surface and during rainfall the air and water surface temperature difference are minimal, although it can be easily relaxed), and consider that the wind velocity, air temperature, and air specific humidity are measured at the same location above the surface, C_H and C_E are given by

$$C_H = \frac{\kappa^2}{\ln\left(\frac{z_m}{z_{0,h}}\right)\ln\left(\frac{z_m}{z_0}\right)}, \tag{20}$$

$$C_E = \frac{\kappa^2}{\ln\left(\frac{z_m}{z_{0,v}}\right)\ln\left(\frac{z_m}{z_0}\right)}. \tag{21}$$

Here, $\kappa = 0.4$ is the von Kàrmàn constant; z_m is the height of the measurement point for air properties; z_0 is the momentum roughness length; $z_{0,h}$ is the thermal roughness length; and $z_{0,v}$ is the water vapor roughness length (m); we assume the displacement height is negligibly small compare to z_m. For a smooth surface like the top surface of the runoff, it is usually assumed that $z_0 \simeq z_{0,h} \simeq z_{0,v} \simeq 9\nu / u_*$, where ν and u_* are the air kinematic viscosity ($m^2 s^{-1}$) and the friction velocity ($m s^{-1}$), respectively (Brustaert, 2013; Pope, 2001). The constant, taken as 9 here, is an empirical parameter that is sometimes reported to have a slightly lower value (down to 7.5), but as long as the same value is used for heat and humidity, the impact on the surface energy partitioning is insignificant. The friction velocity can be estimated assuming the log-law velocity profile in the surface layer for a neutral ABL over a smooth surface (Brustaert, 2013):

$$\frac{u_{air}}{u_*} = \frac{1}{\kappa} \ln\left(\frac{z_m}{9\nu / u_*}\right). \tag{22}$$

Equation (22) should be solved (iteratively) for the friction velocity using the measured u_{air} at height z_m above the surface.

The bottom boundary of the runoff is the interface between the water flow and the ground. Similar to the top boundary, a surface energy budget equation is solved for this bottom boundary to get the ground surface temperature at each time step

$$R_{sw} + Q_{wb} + G = 0, \tag{23}$$

where R_{sw} (W m^{-2}) is the net shortwave radiation (upwelling shortwave – downwelling shortwave); $Q_{wb} = k_w \left(\frac{\partial T_w}{\partial y}\right)_{y=0}$ is the energy flux associated with the heat exchange between the ground surface and the runoff water (no negative sign is used in this expression due to the definition of the heat flux direction in (23)); and $G = -k_g \left(\frac{\partial T_g}{\partial y}\right)_{y=0}$ is the ground heat flux at the ground surface. As for the top surface, all fluxes are defined positive into the surface. Constant diffusive heat flux in the *x* direction is assumed for the left and right boundary conditions of the subsurface domain for equation (9). This condition implies that the heat flux divergence is zero and heat cannot accumulate at these boundaries. Finally, for the bottom boundary of the subsurface, a zero vertical heat flux boundary condition is used.

2.2 Fully pervious pavement

For fully pervious pavements, the entire rainfall infiltrates and no runoff is generated (typical of pervious concrete or porous asphalt pavements made to be highly permeable). To take into account the heat exchange by the infiltrating rain water, a vertical advection term is added to equation (9) (which was used for the impervious pavements):

$$\frac{\partial T_g(x,y,t)}{\partial t} = D_g\left(\frac{\partial^2 T_g(x,y,t)}{\partial y^2} + \frac{\partial^2 T_g(x,y,t)}{\partial x^2}\right) - v_g \frac{\partial T_g(x,y,t)}{\partial y}, \tag{24}$$

where v_g is the infiltration velocity in the subsurface, and can be estimated using the rain intensity and the porosity (φ) of the pavement as

$$v_g = \frac{i}{\varphi}. \tag{25}$$

Similar to the impervious pavement model, we also assume that a thin stationary layer of water above the surface develops when the rain starts, and persists for the rest of precipitation event. It yields a pavement water-holding capacity. This layer fills the surface depressions not connected to the subsurface, and wets the rest of the surface until gravity forces overcome the capillary forces holding the water on the surface. The same heat equation and boundary conditions described previously for the stationary layer above an impervious pavement are used. The thickness of this layer is used as the sole calibration parameter for the pervious pavements model (recall that the effective diffusivity is the main calibration parameter for the heat model of impervious pavements, while the slope is calibrated in the runoff flow model). The applicable (in

the subsurface) boundary conditions for equation (24) are similar to the boundary conditions of the impervious pavement model. Note that at the bottom subsurface boundary of this case, since the temperature gradients are zero, both advective and diffusive heat fluxes vanish.

3 Numerical implementation

In order to obtain numerical solutions for the heat budget equations in the runoff layer (equations (8) and (9)), we need to first solve for runoff depth and velocity (equations (4), (6), and (7)) in the domain, either analytically or numerically. The challenge here lies in the fact that the runoff domain over which we need to numerically solve the heat equation is not a simple rectangular domain, and a uniform mesh grid cannot be used to map it. Therefore, for efficient numerical solution, we transfer the runoff physical domain to a simple Cartesian computational domain. In this transformation, the horizontal coordinate in the computational domain remains the same as in the physical domain (x), but the vertical coordinate is normalized by the local depth of the runoff:

$$\eta = \frac{y}{h}, \tag{26}$$

where η is vertical coordinate of the computational domain (recall that the stagnant layer depth δ is included in both y and h). For an illustration of how this coordinate transformation works, refer to the supporting information section S2. We also need to transform the heat equation for the runoff to the computational coordinates where it becomes:

$$\frac{\partial T_w}{\partial t} = \frac{\partial}{\partial \eta}\left(D_w \frac{\partial T_w}{\partial \eta} \right) \eta_y^2 - \left(u \frac{\partial T_w}{\partial \eta} \eta_x + u \frac{\partial T_w}{\partial x} + v \frac{\partial T_w}{\partial \eta} \eta_y \right). \quad (27)$$

η_y and η_x are the derivatives of η with respect to y and x respectively. The runoff velocity and corresponding boundary conditions also need to be transferred to the new coordinates in a similar way. Note that we do not use the same technique for the subsurface domain since it is rectangular and amenable to Cartesian meshing, and we simply solve the heat equation as given in equation (9) in the subsurface physical domain. However, we align the horizontal mesh grid points in the subsurface and in the runoff layer for easier coupling of equation (27) and (9) at the interface between the runoff and subsurface.

As discussed in the previous section, when the rain starts, first the stationary layer develops, and subsequently the runoff begins according to the runoff depth solution in equation (6). Therefore, the geometry, which we are solving the heat equation for, changes in time until the entire runoff domain conforms to the steady part of equation (6). This requires the use of a dynamic mesh for the period of time when the domain geometry is changing. At each time step, we need to generate a new mesh grid and interpolate (or linearly extrapolate if the grid points in the new mesh are outside the old domain) the previous time step' solutions to the new mesh grid before advancing the heat equations in time on the new mesh. This process should be repeated until the depth of the runoff no longer changes with time, after which a static mesh grid can be used. Some of the numerical details associated with this dynamic mesh are presented in supporting information section S2. For the pervious pavements model, no domain transformation

is needed. However, a dynamic mesh is used for the stationary layer during its initial development.

The numerical discretization of the equation consists of explicit Euler method in time for equations (27), (9), and (24). A second-order central finite difference scheme is used for the second derivatives (diffusion terms), and a first-order upwind finite difference scheme is used for the first derivatives (advection terms). The time step of the numerical simulation is limited by the initial development of the stationary layer during the initial period of the rainfall because this layer is very thin at the beginning. The time step (Δt) limit for the diffusion equation that is solved during this initial time can be obtained by the Von Neumann stability analysis, and it leads to the time step limitation of $\Delta t \leq \Delta y^2 / \left(2D_w\right)$, where $\Delta y^2 / \left(2D_w\right) \simeq 10^{-4}$s in our simulations. To speed up the simulation, a dynamic time step can be implemented to increase its value after the initial development of the stationary layer; however, we used a constant time step of 10^{-4} s in all the simulations reported in this paper because the simulation run time was not an important constraint.

Grid convergence tests were performed with respect to (i) the number of vertical grid points in the subsurface (m_s), (ii) the number of the vertical grid points in the runoff layer (for impervious pavement) or the stationary layer (pervious pavement) (m_r), and (iii) the number of the horizontal grid points (n), which is the same for the runoff and subsurface domains. The grid convergence test process and results for the pervious pavements are detailed in the supporting information section S3. Based on these results (and the tests for the pervious pavements that are not shown),

we adopted $m_r = 5$, $m_s = 25$, and $n = 30$ for both impervious and pervious pavements. These results are for a horizontal length of 3.3 m, subsurface depth of around 8 cm and a maximum runoff depth of 3.7 mm (at the downstream end when the entire runoff is in steady state), and it leads to grid resolutions of 11 cm for the horizontal direction, 3.2 mm for the vertical direction inside the subsurface, and 0.74 mm for the vertical direction in the runoff.

4 Experimental Campaign

The field measurements were conducted at a site near the Arizona State University campus (Coordinates: 33°26'24.8"N, 111°55'25.8"W). The site consists of four different pavement slabs all with length and width of 3.3 m, and a thickness of 15.5 cm: porous Hot Mix Asphalt (HMA), conventional dense (impervious) HMA, porous Portland Cement Concrete (PCC), and impervious PCC (Figure 2a). Each pavement is embedded with 3 thermocouples (accuracy = ± 0.5 ºC) vertically aligned at depths of ≈ 0 (directly below the surface), 7.5, and 15 cm to measure the subsurface temperature. During the experiments, these thermocouples were measuring the temperature every 30 minutes (these were pre-existing instruments that we did not add or tailor for the present experiment), and because the duration of each experiment was less than 30 minutes (around 7 minutes), the data from the embedded thermocouples were used just to estimate the initial temperature distribution of the subsurface for the model validation. All the experiments were conducted under artificial rain generated using spray nozzles (Figure 2c, also see supporting information movie S8). Four flow meters were used to measure the flow rate

going to the spray nozzles, which was then converted to the rainfall intensity using the pavement area.

The longwave and shortwave radiations were measured by a 4-component radiometer (NR01-L, Campbell Scientific, with an accuracy of about 10%). A Vaisala weather transmitter (WXT520 with accuracy of ±1 hPA for pressure, ±0.3ºC for air temperature, ±3% at 10 m/s for wind speed, and ±3% for relative humidity) was used to measure the air properties i.e. temperature, relative humidity, pressure, wind speed (Figure 2d). A water content reflectometer (CS616, Campbell Scientific) sensor was repurposed and calibrated to measure runoff depth for the experiments on the impervious pavements (Figure 2b). To measure the ground surface temperature, a type T thermocouple (Omega Engineering, accuracy = ±0.5 ºC) was attached to the surface for all the experiments.

To measure the temperature inside the runoff, a set of type K (accuracy = ± 1 ºC) thermocouples was aligned vertically inside a 3-D printed hydrofoil (Figure 2b). The first two (out of 8) thermocouples in the box were at 2 and 4 mm above the ground. Because for the experiments on the impervious pavements, it was observed that only the first (lowest) thermocouple was entirely submerged in the runoff (after the runoff depth reaches to 2 mm), we primarily used the measurement of this thermocouple in the model validation.

A CR3000 Campbell Scientific data logger was used for data collection of all the sensors (Figure 2c). All the measurements were collected at 20 Hz except the air measurements from WXT520, which were collected at 1 Hz. The 20 Hz data were averaged in post-processing to 1

Hz data since this was found to be a sufficient resolution. For the experiments on the impervious pavements, the entire measurement setup was placed at the downstream end of the runoff (it varies between the pavements and depends on the average slope of the pavement). Figure 2c also shows the measurement setup for the experiment over the impervious concrete. The experiments on the pervious pavements (without runoff) were similar to the ones on impervious pavements except that there was no need to measure the runoff depth or temperature (refer to the supporting information for a video of experiments over pervious pavement). All the experiments were conducted during clear sky conditions. Although some of the fluxes (such as shortwave radiation) might then be higher than is expected during real rainfall events, the model (runoff + heat budgets) can still be validated. In the last section, we use meteorological data collected during a rainfall event to investigate the heat transfer dynamics under realistic rainfall conditions.

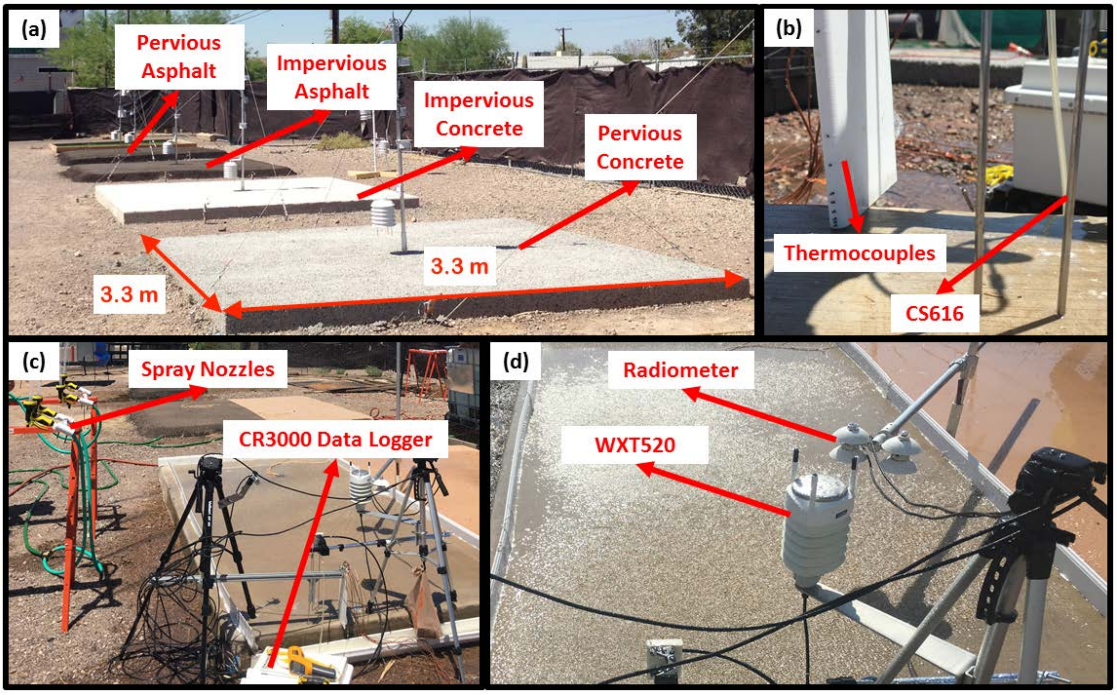

Figure 2. Experimental site and sensors. (a) the 4 types of pavements used (picture not from the present experiment: no stations were placed in the middle of each pavement), (b) the 3D printed hydrofoil with embedded thermocouples and the water depth sensor (CS616), (c) view of full set of instruments with the spray nozzles generating rain, and (d) the radiometer and WXT520 weather transmitter with a view of the runoff and rainfall impact.

The thickness of the stationary layer for the impervious pavements was measured and found to be ≈ 0.5 mm for both impervious pavements (see method and illustrative figures in the supporting information section S5). The rain temperature was measured by the top 4 thermocouples in the 3D printed box. These thermocouples were constantly receiving rainfall during each experiment. For all of the experiments, the water inside the hoses was initially at a higher temperature than the water in the tanks because the hoses were under the sun during the

experiments and the air temperature reached up to 48 ºC; however, the rain temperature eventually decreases to the tank temperature. While we avoided the very hot initial water, since we were not able to ensure that when we turned the artificial rainfall onto the pavement we had a constant temperature, we fitted an exponential curve between the initial temperature of the rain (T_i) when it was targeted toward the pavement (start of experiment) and the final tank temperature (T_f) using measurements from the topmost thermocouples in the hydrofoil to calculate the rain temperature time series as an input for the model following:

$$T_r = T_f + \left(T_i - T_f\right)e^{-\lambda t} \tag{28}$$

where λ is calculated for each experiment separately.

5 Model validation

In this section, the simulation results of the model introduced in section 3 are compared with the field measured data described in section 4. We categorize the model inputs into four groups: (1) thermal and geometric properties of experimental pavements (see Table 1), (2) thermal properties of rain water and air (all the values are taken at 20 ºC and listed in Table S1 in the supporting information), (3) calibration parameters that will be discussed in section 5.1, and (4) the meteorological variables measured by different sensors such as air temperature, humidity and pressure, wind speed, upwelling and downwelling shortwave radiation, downwelling longwave radiation, rain temperature and intensity, and initial ground surface and subsurface temperature.

For all of the model validation figures in this section, the start time t=0 zero is when the rainfall starts and the plots are shown until the rainfall stops. As mentioned in section 4, to measure the ground surface temperature, a thermocouple was attached to the surface near the downstream end of the pavements (ground thermocouple). Since the exact distance of this thermocouple from the leading edge of runoff initiation could not be measured precisely in the experiments, we compared its measurements to the averaged simulated surface temperature of last quarter of the pavements (where the temperature did not change significantly along the streamwise direction). Hence, in this section, whenever we mention the ground surface temperature in the model, it refers to the averaged ground surface temperature of last quarter of the pavements

5.1 Calibration parameters

The impervious pavements model has two calibration parameters: pavement slope for the runoff model, and the effective diffusivity constant (β) in equation (12) for the heat budget model. We measured the slope of each impervious pavements and it varied significantly along the measurement area (for the impervious concrete the slope was in the range of 0.06-0.56 %, and for the impervious asphalt it was in the range of 0.3-2.4 %). Therefore, we chose the values for the pavements slope that yield a modeled depth at the downstream measurement point (when it is in steady state) that best matches the experimental measurements. Values of 0.15 % and

0.4 % were determined for the slopes of impervious concrete and asphalt, respectively. Both of these calibrated values are within the ranges of slopes measured over these two pavements.

Figure 3 shows the effect of β in equation (12) on the ground surface temperature and the temperature of the runoff at 2 mm above the ground. To choose the suitable value for β, we calculated the Root Means Square Error (RMSE) of the model result relative to a smoothed version of the experiment data for both surface temperature (RMSE1) and the temperature of the runoff at 2 mm (RMSE2). The smoothing of the experimental data is useful to filter out the effect of ripples that formed on the water surface (due to raindrop impact and to wind variability) and that could not be captured in the model. We found that for β = 4, the sum of RMSE values (RMSE1+RMSE2) is the smallest; therefore, we adopt this value for the rest of this paper. Given this finite value of β, and the differences between ground surface and water temperature at 2 mm that persist till the end of the run, the assumption that the water layer is in thermal equilibrium with the surface (equivalent to having an infinite β) is not generally justified especially for short rainfall duration. For longer rainfall events, this assumption might be more acceptable as we will show in the case study (section 6). But even for longer events, the temperature difference between the ground surface and runoff can remain significant over long pavements, at the downstream end).

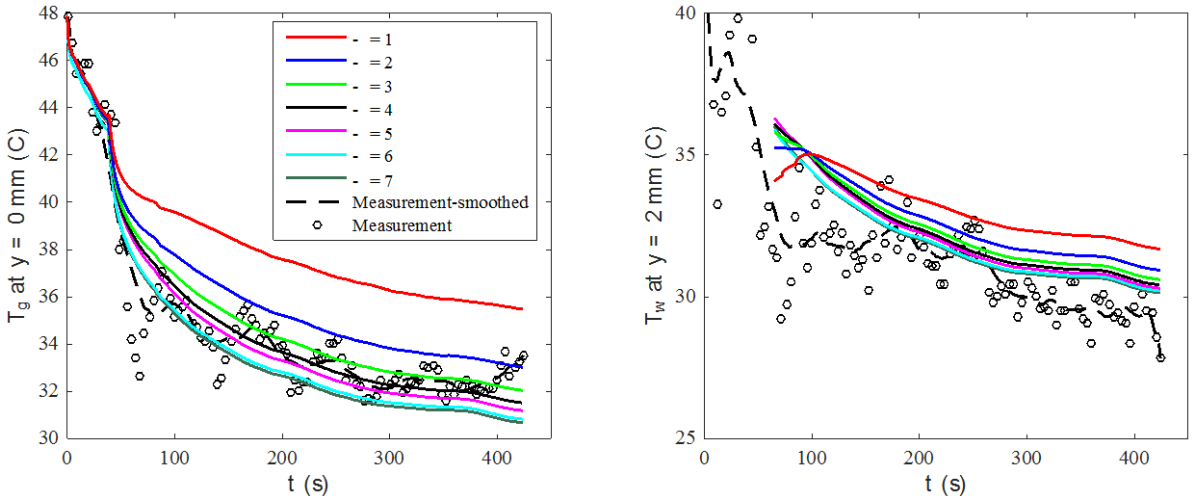

Figure 3. Effect of the mixing factor β on the ground surface temperature (left), and runoff temperature at 2 mm above the ground (right)

For the pervious pavement model, the only calibration parameter is the pavement surface water holding capacity, for which a value of 1 mm is found to yield the best agreement with the observations for both pervious pavements. Note that this value is greater than the measured value of 0.5 mm for the impervious pavements, and according to Figure 4 it is an expected outcome because the pervious pavements have larger roughness than the impervious ones.

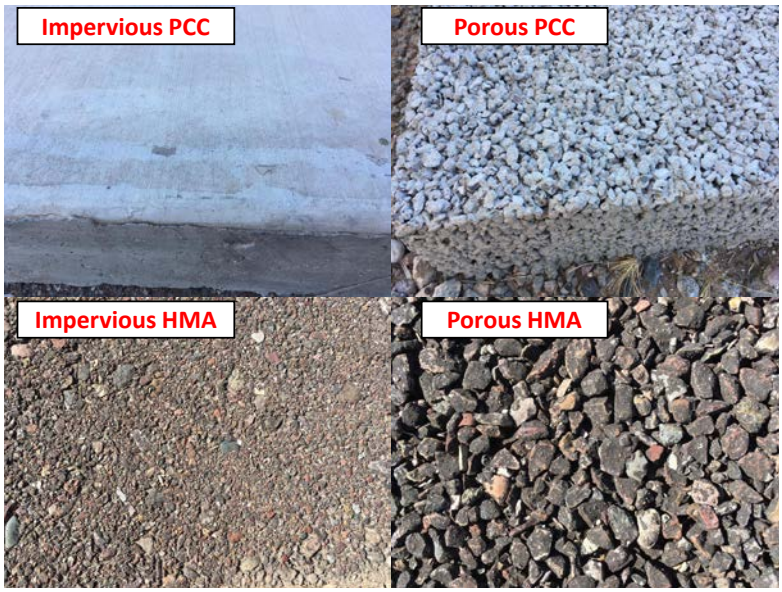

Figure 4. Comparison of the roughness for the impervious and pervious pavements of the measurement field. HMA is Hot Mix Asphalt and PCC is Portland Cement Concrete (PCC).

5.2 Validation: impervious pavements

Figure 5 shows how the downstream runoff depth changes during rainfall for both impervious pavements. One can notice the good agreement between the experimental data and the model results (RMSE for the asphalt and concrete cases are 0.55 and 0.59 mm respectively). For both cases and as explained earlier, the runoff does not start immediately when rainfall begins due to the pavement water holding capacity. Subsequently, the downstream runoff depth increases as expected from equation (6) until the entire pavement reaches steady state, after which the depth remains constant till the end of the precipitation event. At the beginning of each experiment, there was some uncertainty in estimating the exact rainfall start time and intensity due to the

need to aim the water nozzles onto the pavement, manually, as a function of the wind direction and speed. Therefore, we adjusted the rainfall intensity at the beginning of each experiment, before runoff begins, by matching the time needed for the initial stationary layer to fill up in the model and experiments.

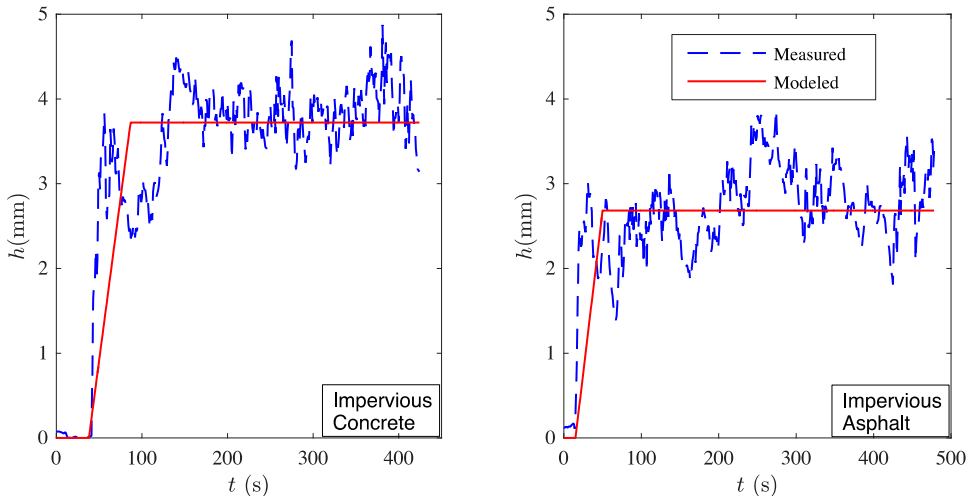

Figure 5. Downstream runoff depth from the model output and the observations for impervious concrete (left), and impervious asphalt (right)

Figure 6a and Figure 6b show the ground surface temperature versus time for the impervious pavements. Again, there is a good agreement between the model and the experimental data (collected by the thermocouple attached to the ground surface) for both cases with RMSE values of 1.3 and 1.7 ºC for the concrete and asphalt respectively. For both surfaces, a large temperature drop of about 15 ºC is observed during the simulated rain event, although we should point out that the tests were not conducted at the same time or with the same initial conditions. The validation results for the runoff water temperature (at 2 mm from the ground, first thermocouple

in hydrofoil) are depicted in Figure 6c and Figure 6d. Good agreement is noted for this variable as well for both impervious pavements with RMSE values 1.9 ºC for the concrete case, and 1.8 ºC for the asphalt case (the comparison begins when the downstream runoff depth reaches 2 mm and the first thermocouple is submerged). Figure 6e and Figure 6f show the difference between the ground surface and runoff temperature at 2 mm from the ground for concrete and asphalt respectively. It can be noted that for both cases the ground surface temperature remains at least 1 ºC hotter than the runoff temperature during the rainfall. This temperature difference persists here despite the high rainfall rate, and is larger for concrete than for asphalt since concrete's higher conductivity allows the surface to extract a higher heat flux from the subsurface. The underestimation by the model of the surface-water temperature difference for concrete is hence probably due to an underestimation of the material's thermal conductivity or effusivity.

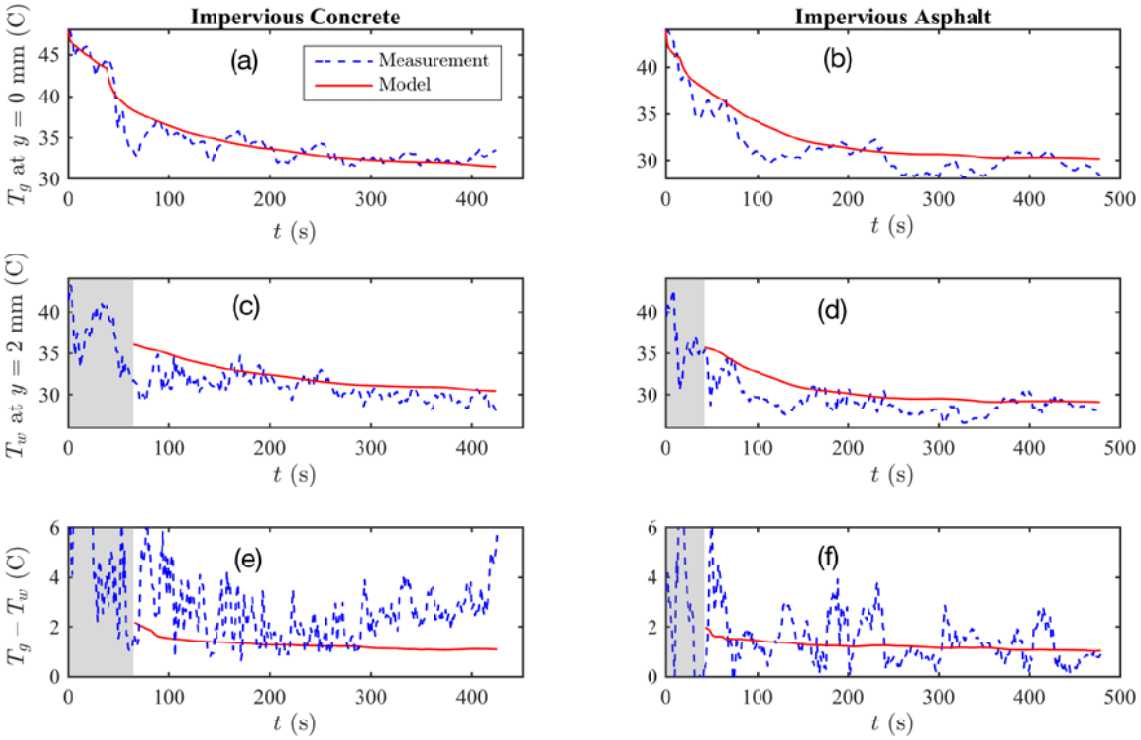

Figure 6. Ground surface temperature (top panel), runoff temperature at 2 mm above the ground (middle panel), difference between ground surface and runoff temperature at 2 mm (bottom panel) from the model and the observations for impervious concrete (left panel), and impervious asphalt (right panel).

5.3 Validation: pervious pavements

Similar to the impervious pavement cases, we validated the pervious pavement results for the ground surface temperature using the data measured by the thermocouple attached to the ground for both pervious pavements. In this case, there is no runoff temperature to validate. Figure 7 shows very good agreement between the model and experimental results for both surfaces (with RMSE values of 1.5 ºC and 1.0 ºC for previous concrete and asphalt respectively). Similar to the

impervious pavements, one can observe a large temperature drop (15 ºC for the concrete and 14 ºC for the asphalt) during the rainfall in both tests.

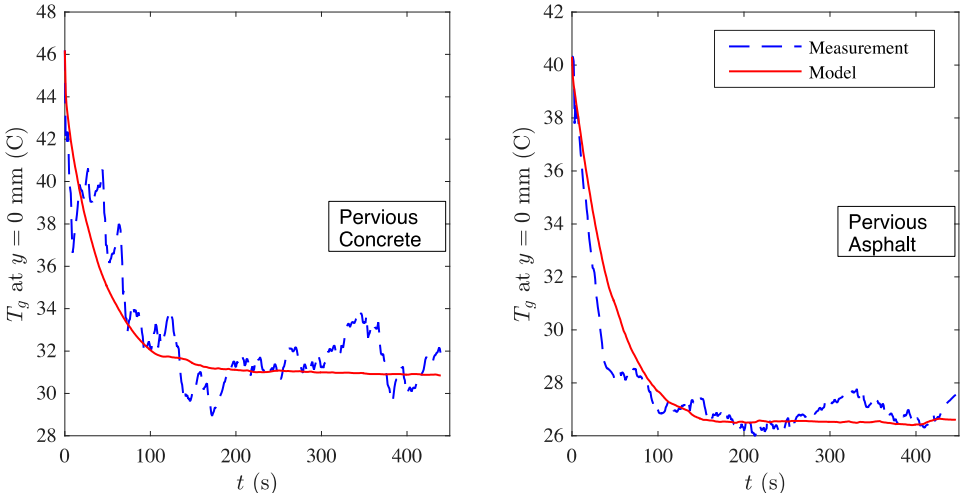

Figure 7. Ground surface temperature from model output and the observations for pervious concrete (left), and pervious asphalt (right)

6 Parking lot case study: impervious versus pervious pavements

The model developed and validated above can be used to investigate the thermal dynamics of pavement cooling under rainfall and to predict runoff water temperature. Here, we perform an application for illustration purposes, and more importantly to start addressing the broader aims of this effort of understanding the processes controlling heat transfer from hot surfaces and how the surface and runoff temperatures evolve during a rainfall event. We design a hypothetical parking lot for our case study since most parking lots are made of dense asphalt concrete or Portland cement concrete material, which can absorb a large amount of heat during the day. A daytime

rainfall event can thus extract this heat (by runoff or infiltration) and advect it into the streams directly or through drainage networks. Our model can elucidate the heat transfer mechanisms and magnitude in the pavement and runoff during rainfall.

A 50 m long by 50 m wide (although cross-stream width is not consequential) parking lot is considered with two scenarios: the lot area is fully covered with (i) impervious paving material (no infiltration), or (ii) fully pervious material (no runoff). The same rain and air thermal properties used for the validation are adopted (Table 1 and Table S1 in the supporting information). The parking lot surface is dry before the rain starts for both scenarios. As discussed before, various atmospheric data are needed as inputs. Since the data collected in Arizona was during an unusually hot period under sunny conditions that do not resemble the atmospheric conditions during rainfall, and to have a more representative application, we use climatic measurements at the Broadmead station at Princeton University (coordinates: 40°20'46.9"N, 74°38'36.5"W, more details are provided in Ramamurthy et al. [2014]). A real precipitation event on 30 July 2016 is chosen for this case study. This rainfall event is perfectly suited for the case study because precipitation starts around 2 pm local time with no rainfall before, meaning that the initial temperature of the pavements is high. The total duration of the case study here is 3 hours. The original data set has a 5-minute temporal resolution; we thus interpolated the data to 1 Hz to use it as the input for the model. The upwelling shortwave radiation is calculated using an assumed albedo of 0.05 for both impermeable and porous cases, and rain temperature is assumed to be equal to the air temperature during the rainfall.

The initial temperature of the pavement surface, as well as the temperature profile in the subsurface before the rainfall event, are computed using the time-varying atmospheric input data for the 12-hour period preceding the rain event. The surface and subsurface temperatures are solved for by combining the surface energy budget equation for the dry pavement surface and the heat conduction equation for the subsurface, using the same methodology as before, but without any rain or runoff and with no evaporation. After rainfall begins, we assume a constant in time and uniform along the pavements rain intensity, which is set equal to the measured intensity of 30 mm h^{-1} (this is the highest intensity we can use for such a large parking lot without the flow becoming turbulent, a regime that cannot be captured by the present model).

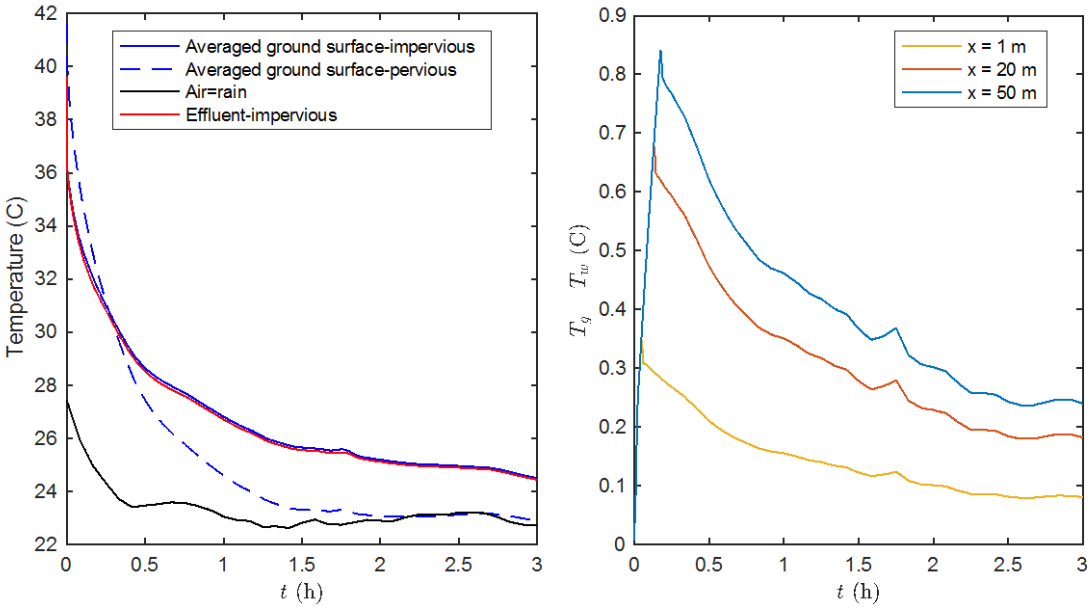

Figure 8. Left: averaged (along the pavement) ground surface, air (= rain) , and vertically-averaged effluent temperature time series (at downstream). Right: time evolution of the difference between ground surface and water surface temperature values for x = 1 m, x = 20 m, and x = 50 m.

Figure 8a shows the result of the averaged (along the entire pavement length) ground surface temperature for both impervious and pervious pavements during the 3 hours of rainfall (see supporting information for runoff and subsurface temperature contours animation, movie S7). Both surfaces cool rapidly, and much more significantly than the air (notice that air cooling is entirely based on observations). The rate of surface cooling is high at the beginning of the rainfall event for both cases, but it slows down as thermal equilibrium between rainfall and surface is approached. Although the pervious pavement has a higher (by about 2ºC) initial

ground surface temperature than the impervious one, after 3 hours of rainfall, the surface temperature of the pervious pavement is in equilibrium with the rain temperature and 1.5 ºC lower than the impervious surface. This implies that the average rate of cooling of the surface temperature for the pervious pavement is higher than the impervious case. In addition, Figure 8a shows the vertically-averaged effluent temperature at the end of the domain (downstream). During the entire 3 hours of rainfall, the impervious effluent temperature is higher than the rain temperature (by 12 ºC at the beginning of the event, and 1.5 ºC at the end), which is the result of heat extraction form the subsurface by the runoff. As discussed earlier, this hot runoff will eventually merge with the streams and result in adverse impacts on their temperature and consequently on their ecology. One should bear in mind that in the pervious pavement case, if the infiltrated water eventually reaches an impervious bed layer, it can also flow towards the streams. Since it can extract even more thermal energy from the subsurface because it travels deeper into the ground subsurface, its thermal pollution impacts might potentially be higher than that of the impervious pavement.

Figure 8b shows the time series of temperature difference between the ground surface and runoff surface ($T_g - T_w$) for different horizontal positions along the pavement (x =1, 20, 50 m). This figure indicates that for each specific horizontal position, the temperature difference increases at the beginning during the time when the runoff is unsteady at that location since a new water layer builds up there on top of the runoff. However, as the runoff approaches a steady

state, $T_g - T_w$ starts decreasing. From Figure 8b, we can note that for a specific duration of the rainfall, $T_g - T_w$ is higher downstream compared to upstream since the runoff depth is larger. The difference is also larger for short rainfall duration. In general, this temperature difference between ground surface and runoff surface can be significant enough to make the thermal equilibrium assumption questionable (even for very short duration rainfall, the temperate difference can be large for short pavements as we showed in Figure 6). It illustrates the benefit of the full model developed here that can assess the departure from thermal equilibrium.We can gain further insight into the difference between these two parking lots by looking at the different terms in the surface energy budget equations. Figure 10 shows the time series (averaged along the pavement length) of these terms for the ground surface, equation (23), and the water surface, equation (13) (runoff surface for the impervious pavement case, and stationary water layer for the pervious case). Remember that a positive flux value means that the flux goes into the surface (or heats the surface). For the ground surface energy budget, shortwave (R_{SW}) and ground heat flux (G) are the positive terms that heat the surface, and the heat exchange between the ground surface and the water is the cooling term for both impervious and pervious pavements, as expected. Both surfaces have the same value of the shortwave radiation because the same downwelling shortwave and albedo were imposed, but this shortwave component is small due to the cloudiness during rainfall. The ground heat flux for the pervious pavement is higher than for the impervious one at the beginning of the rainfall; this is related to the higher initial ground surface temperature of the pervious pavement that must transfer more energy to the water layer.

However, as the subsurface and ground cool down, G decreases faster in the pervious pavement to reach 0, whereas over the impervious one it maintains a value of about 70 W m^{-2} at the end of the 3-hour rainfall event. The larger absolute value of Q_{wb} (larger vertical temperature gradients in the water layer and immediately above the ground surface) at the beginning of the rainfall (500 and 760 W m^{-2} for the impervious and pervious asphalt, respectively) in comparison to the end of rainfall is another indicator of the approach to thermal equilibrium between runoff (impervious) or stationary water layer (pervious) layers and the ground surface.

Among the water top surface energy budget components, the main term heating the surface is the heat exchange between the water surface and the water below it (Q_{wt}), and the main terms cooling the surface are the net flux of cooler rainfall (Q_r) and the evaporation (LE_e) (H, and R_{lw} also cool the surface but their values are much smaller than Q_r and LE_e). At the beginning of the rainfall, the evaporation rate is higher for the pervious pavement than the impervious one because of initially higher pervious ground surface temperature, but the two converge at later times.

From Figure 10, one can construct a detailed understanding of how heat is primarily transferred between the pavement and water layer during a rainfall event. Considering an impervious pavement, (1) heat is being transferred from the subsurface to the ground surface through G, (2) G and shortwave radiation (positive values) heat the ground surface, (3) Q_{wb} (negative value) cools down the ground surface by transferring heat to the runoff by diffusion, (4) then a fraction of this heat is advected by the runoff while the remainder is transferred to the

water surface by diffusion to heat the water surface (in conjunction with downwelling longwave), (5) this heating of the water surface balances its cooling mainly by the rainfall and evaporation. The other heat transfer mechanisms play a secondary role. Similar processes are in play over a pervious pavement but (i) the subsurface cools down by the infiltration, and (ii) Q_{wb} is transferred only by diffusion through the stationary water layer at the surface. For the pervious pavement, $Q_{wb} \approx -Q_{wt}$, and that energy goes to balance the radiative and evaporative cooling while the vertical downward advection of heat by the infiltrating water is the primary mechanism of heat removal from the surface. Another important observation from this figure is that while the pervious pavement seems to equilibrate in about 1.5 hours, the impervious one is still evolving (with a lower rate of temperature change) even after 3 hours of rainfall.

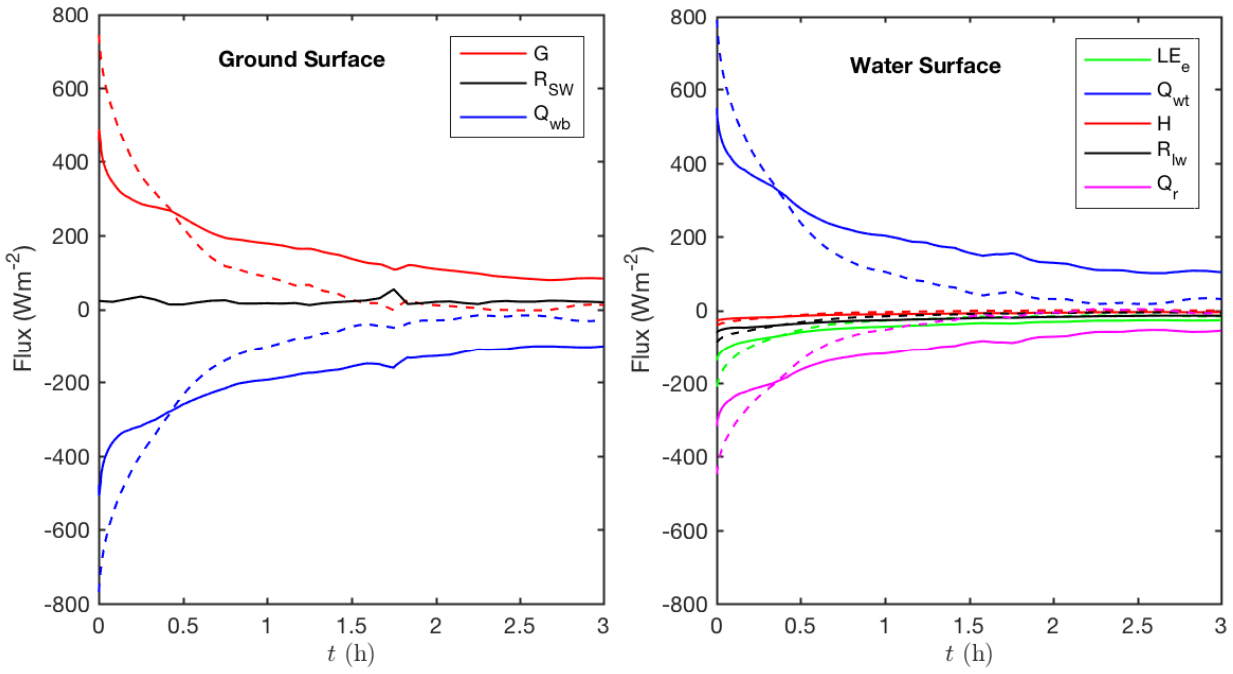

Figure 9. Time series of the surface energy budget terms of the ground surface (left) and water surface (right) for the impervious (solid line) and pervious (dashed line) pavements.

To examine the thermal budget of the whole water layer for the impervious pavement, Figure 10 depicts the time series of bulk heat fluxes contributing to the heat budgets of the water layer during the rainfall. These fluxes are $-Q_{wb}$, $-Q_{wt}$, and $Q_{adv} = \rho_w c_w \left(iT_{ws} - \int_0^h \frac{u_{eff} T_{eff}}{l} dy \right)$, which is the net advective flux of the water layer defined positive out of the layer unlike the other fluxes (water entering the control volume at the temperature T_{sw}, and leaving it with the effluent velocity u_{eff} and temperature T_{eff}). Notice that the effluent term is normalized by the pavement length so it is equivalent to surface fluxes. In addition, in Figure 10 we also plot the sum of these fluxes, which is approximately equal to the tendency term for the runoff average temperature, $Q_t = \rho_w c_w \frac{\partial \overline{h \langle T_w \rangle_y}}{\partial t}$, where $\langle T_w \rangle_y$ is the vertically-averaged runoff temperature and the overbar indicates averaging in the streamwise direction. The sum of the fluxes is a large positive number (around 1200 W m^{-2}) during the development of the runoff (i.e. before the runoff over the entire pavement reaches a steady state). During this period, thermal energy is accumulating as the water depth increases; although T_w decreases in time, h increases and overall $\overline{h \langle T_w \rangle_y}$ increases leading to a positive tendency term (Q_t or $-Q_{wb}-Q_{wt}+Q_{adv}$). However, as the runoff over the entire pavement approaches steady state (and h becomes constant in time), Q_t plateaus to a small

negative number indicating that the runoff is close to thermal equilibrium with the pavement, and the averaged runoff temperature slowly decreases in time. During that period, $Q_{wb} \approx -Q_{wt}$. To assess the thermal pollution resulting from the runoff, we compute the difference between the heat flux that flows to streams with the runoff effluent ($\rho_w c_w i T_{eff}$) and the heat that would have resulted if the rainfall had entered the stream without heating over the pavement ($\rho_w c_w i T_r$). This value, $\Delta Q_{runoff} = \rho_w c_w i (T_{eff} - T_r)$, is in fact the net amount of heat rainfall picks up over the pavement and is shown in Figure 10. It reaches a maximum value of around 240 W m^{-2}, and plateaus to 60 W m^{-2} after 3 hours of rainfall. These are large numbers and for small streams will cause a significant thermal shock.

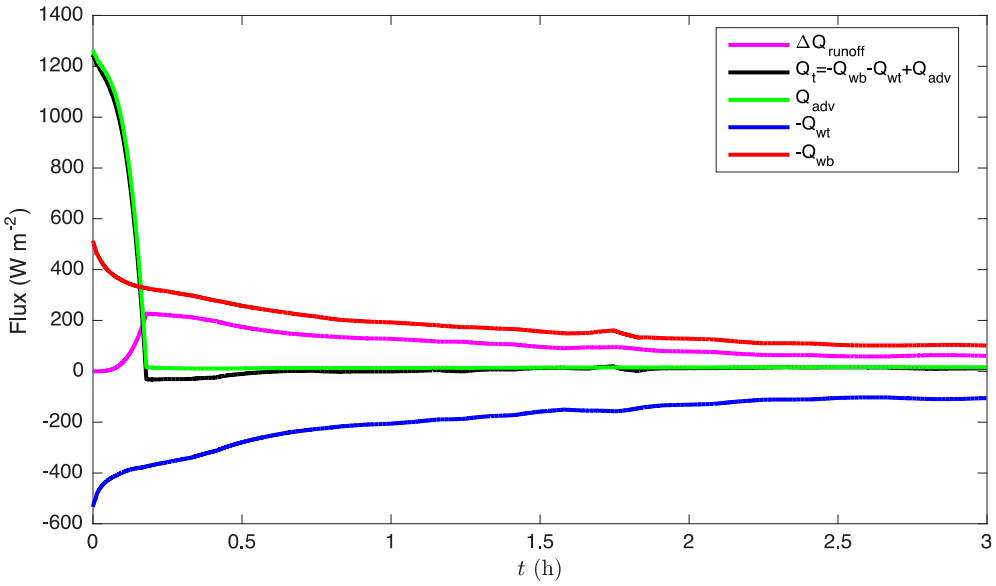

Figure 10. Time series of different terms in the thermal budget of the whole water layer for the impervious parking pavement.

7 Model limitations

The model as formulated here has some limitations that are important to appreciate, but that can be eliminated in future developments:

(i) *Turbulent flow*: Longer pavement length leads to an increase in the runoff velocity. Therefore, for long pavements, there will be a transition to a turbulent regime at some distance from the starting point. The current model does not account for that transition and cannot simulate turbulent flows. Turbulence in runoff increases momentum and thermal mixing (in addition to the mixing by rain droplets), which leads to more rapid cooling/heating of the pavement/runoff. To account for turbulent mixing, a turbulence closure scheme is being added to the model to account for turbulence modification of runoff dynamics as well as heat transfer processes inside the runoff.

(ii) *Rain droplet effects on the runoff dynamics*: when we derived the runoff dynamics equations in section 2.1.1, for simplicity, it was assumed that the rain droplets penetration inside the runoff does not have any effect on the momentum budget. However, what will actually happen is that the rain droplets fall on the runoff with a zero horizontal momentum and this will result in drag at the top surface of the water layer (Yoon & Wenzel, 1971), slowing down the runoff and increasing the runoff depth for a certain rain intensity. To take into account the rain droplets effects on the runoff dynamics, one can solve a full momentum equation with the consideration of rain droplets streamwise momentum in the equations.

(iii) *Heterogeneous pavements slope*: it was assumed that the slope is constant along the pavements, and this assumption is not necessarily true for pavements in the real world. The slope can change drastically, especially for the very long pavements. In this case, it is possible to use an average value for the slope. Alternatively, the kinematic wave model for runoff can be solved numerically to accurately capture changes in slope when they are significant (we implemented such a solution but do not detail it since it is not used here).

(iv) *Subsurface composition*: The subsurface was assumed to be made of the same material as the surface, which is acceptable for short rainfall periods when the cooling effect remains shallow. For longer events, a more realistic multi-layer subsurface can be simulated with the current model without any further development. In addition, pavements can contain salts or other impurities that can modify the evaporation rate and dynamics (Shokri-kuehni et al., 2017). The current model can be extended to take this modification into account.

8 Conclusion and outlook

An accurate prediction of the earth surface temperature is essential due to its implications on a variety of phenomena in the hydrosphere, the atmosphere, and other earth systems. Here, we developed and validated a model that can capture and predict the rapid cooling of hot urban surfaces during rainfall, elucidate the role of different thermal transport processes, and assist in designing urban infrastructure that minimizes adverse environmental impacts. The model couples runoff or infiltration dynamics with thermal transport physics, and can be applied over

pervious or impervious pavements. A comparison of these two types of pavements was conducted for a hypothetical parking lot, showing significant differences in the response and impacts of pervious and impervious human-made surfaces, and illustrating how the model can be used for urban design. The model results also confirm the premise of this work: runoff can be more than 10 ºC hotter than rainfall and if allowed to drain rapidly into streams will cause adverse impacts.

This is the most detailed model of runoff cooling to be proposed yet, and this paper's focus was on the formulation and validation. The application in this paper nevertheless already gives valuable insight on the dominant physical processes that need to be included in reduced versions. Furthermore, with this detailed model, we are able to test the validity of different assumptions that were included in the previous studies. One main assumption we tested is the existence of thermal equilibrium between the pavement and runoff; our detailed model showed that the temperature difference between ground surface and runoff can be significant for long pavements (as the runoff depth is larger than the upstream) and/or for short duration of rainfall. This thermal disequilibrium is also larger for concrete pavements, compared to asphalt, due to their higher thermal conductivity and effusivity. The model also indicated that the driving thermal transfer processes for the bulk runoff layer are heat gain from the surface and heat loss by the net inflow of colder rainfall and outflow of hot runoff (the later is not captured in the surface schemes used in earth systems models). Latent heat cooling was a secondary - but non-negligible - contributor, while net radiation and sensible heat flux were insignificant under realistic, cloudy rainfall

conditions. More work is underway to further use the present model as a benchmark for developing and testing equivalent models of reduced complexity that can be efficiently embedded in coarse geophysical models such as WRF (i.e. embedded in the Urban Canopy Models in WRF, e.g. (Wang, Bou-Zeid, Smith, & Wang, 2013)). These geophysical models compute atmospheric properties and provide them to their surface modules so all input data needed by our model would be accessible. For offline applications like the ones in this paper, measured meteorological data would be required.

An important next step the authors are undertaking is to conduct a sensitivity analysis of the model to different pavement and atmospheric parameters. This will enable us to investigate the effects of pavements characteristics (such as pavement heat conductivity, slope, etc.) and meteorological properties (such as air and rain temperature) on the cooling or heating processes of the problem. The outcome would allow us to document how design parameters affect urban pavement impacts so readers can apply our findings to urban design without necessarily implementing and running the model.

9 Acknowledgments

This work is supported by the Army Research Office under contract number W911NF-15-1-0003 (program Manager Julia Barzyk) and by the US National Science Foundation's Sustainability Research Network Cooperative Agreement 1444758. The Broadmead atmospheric data were collected and provided to the authors by James A. Smith and Mary Lynn Baeck. The

pavements test slabs were installed at the yard of Creative Paving Solutions, Tempe, Arizona with collaboration with the National Center of Excellence for SMART Innovation at Arizona State University. The authors are also thankful of Chenghao Wang for his assistance in the experimental campaigns.

All experimental data used in this paper are available in the supporting information section (file 2017WR022241-DS01.zip).

References

Angel, S. (2012). *Planet of Cities*. Cambridge, MA: Lincoln Institute of Land Policy.

Bounoua, L., Zhang, P., Mostovoy, G., Thome, K., Masek, J., Imhoff, M., … Toure, A. M. (2015). Impact of urbanization on US surface climate. *Environmental Research Letters*, *10*(8), 84010. https://doi.org/10.1088/1748-9326/10/8/084010

Brustaert, W. (2013). *Evaporation into the atmosphere, theory, history and application* (Vol. 1). Springer Science & Business Media.

Brutsaert, W. (1975). On a derivable formula for long-wave radiation from clear skies. *Water Resources Research*, *11*(5), 742–744.

Brutsaert, W. (2005). *Hydrology: An Introduction*. New York, NY, USA: Cambridge University Press.

Cohard, J.-M., Rosant, J.-M., Rodriguez, F., Andrieu, H., Mestayer, P. G., & Guillevic, P. (2017). Energy and water budgets of asphalt concrete pavement under simulated rain events. *Urban Climate*. https://doi.org/https://doi.org/10.1016/j.uclim.2017.08.009

de Arellano, J. V.-G., Van Heerwaarden, C. C., Van Stratum, B. J. H., & Van Den Dries, K. (2015). *Atmospheric boundary layer: Integrating air chemistry and land interactions*. Cambridge University Press.

Engineering ToolBox. (2017). The Engineering ToolBox. Retrieved from http://www.engineeringtoolbox.com/water-thermal-properties-d_162.html

Ferguson, G., & Woodbury, A. D. (2007). Urban heat island in the subsurface. *Geophysical Research Letters*, *34*(23), 2–5. https://doi.org/10.1029/2007GL032324

Grimmond, S. (2007). Urbanization and global environmental change: local effects of urban warming. *The Geographical Journal*, *173*(1), 83–88. https://doi.org/10.1111/j.1475-4959.2007.232_3.x

Hale, G. M., & Querry, M. R. (1973). Optical Constants of Water in the 200-nm to 200-microm Wavelength Region. *Applied Optics*, *12*(3), 555–563. https://doi.org/10.1364/AO.12.000555

Herb, W. R., Janke, B., Mohseni, O., & Stefan, H. G. (2009). Runoff Temperature Model for Paved Surfaces. *Journal of Hydrologic Engineering*, *14*(10), 1146–1155. https://doi.org/10.1061/(ASCE)HE.1943-5584.0000108

Janke, B. D., Herb, W. R., Mohseni, O., & Stefan, H. G. (2009). Simulation of heat export by rainfall-runoff from a paved surface. *Journal of Hydrology*, *365*(3–4), 195–212. https://doi.org/10.1016/j.jhydrol.2008.11.019

Kertesz, R., & Sansalone, J. (2014). Hydrologic Transport of Thermal Energy from Pavement. *Journal of Environmental Engineering*, *140*(8), 4014028. https://doi.org/10.1061/(ASCE)EE.1943-7870.0000831

Kim, K., Thompson, A. M., & Botter, G. (2008). Modeling of thermal runoff response from an asphalt-paved plot in the framework of the mass response functions. *Water Resources*

Research, *44*(11), 1–13. https://doi.org/10.1029/2007WR005993

Krause, C. W., Lockard, B., Newcomb, T. J., Kibler, D., Lohani, V., & Orth, D. J. (2004). Predicting influences of urban development on thermal habitat in a warm water stream. *Journal Of The American Water Resources Association*, *40*(6), 1645–1658. https://doi.org/10.1111/j.1752-1688.2004.tb01612.x

Lowe, P. R. (1977). An Approximating Polynomial for the Computation of Saturation Vapor Pressure. *Journal of Applied Meteorology*. https://doi.org/10.1175/1520-0450(1977)016<0100:AAPFTC>2.0.CO;2

Monin, A. S., & Obukhov, A. M. (1954). Basic laws of turbulent mixing in the surface layer of the atmosphere. *Contrib. Geophys. Inst. Acad. Sci. USSR*, *24*(151), 163–187.

Nelson, K. C., & Palmer, M. A. (2007). Stream temperature surges under urbanization and climate change: Data, models, and responses. *Journal of the American Water Resources Association*, *43*(2), 440–452. https://doi.org/10.1111/j.1752-1688.2007.00034.x

Oke, T. R. (1973). City size and the urban heat island. *Atmospheric Environment Pergamon Pres*, *7*, 769–779. https://doi.org/10.1016/0004-6981(73)90140-6

Oke, T. R. (1982). The energetic basis of the urban heat island. *Quarterly Journal of the Royal Meteorological Society*, *108*(455), 1–24. https://doi.org/10.1002/qj.49710845502

Parlange, J. Y., Rose, C. W., Sander, G. C., Campbell, S. Y., & Barry, D. A. (1983). Kinematic flow approximation to runoff on a plane: An approximate analytic solution. *Journal of Hydrology*, *62*(1–4), 363–369. https://doi.org/10.1016/0022-1694(83)90113-0

Phelan, P. E., Kaloush, K., Miner, M., Golden, J., Phelan, B., Silva Iii, H., & Taylor, R. A. (2015). Urban Heat Island: Mechanisms, Implications, and Possible Remedies. *Annu. Rev. Environ. Resour*, *40*, 285–307. https://doi.org/10.1146/annurev-environ-102014-021155

Pope, S. B. (2001). Turbulent flows. Cambridge, UK: Cambridge University Press.

Pourshams-Manzouri, T. (2013). *Pavement Temperature Effects on Overall Urban Heat Island, PhD thesis*. Arizona State University, AZ, USA. https://repository.asu.edu/items/17862.

Ramamurthy, P., & Bou-Zeid, E. (2014). Contribution of impervious surfaces to urban evaporation. *Water Resources Research*, *50*, 2889–2902. https://doi.org/10.1002/2013WR013909

Ramamurthy, P., Bou-Zeid, E., Smith, J. A., Wang, Z., Baeck, M. L., Saliendra, N. Z., … Welty, C. (2014). Influence of subfacet heterogeneity and material properties on the urban surface energy budget. *Journal of Applied Meteorology and Climatology*, *53*(9), 2114–2129. https://doi.org/10.1175/JAMC-D-13-0286.1

Sansalone, J. J., & Teng, Z. (2005). Transient rainfall-runoff loadings to a partial exfiltration system: Implications for urban water quantity and quality. *Journal of Environmental Engineering-Asce*, *131*(8), 1155–1167. https://doi.org/10.1061/(ASCE)0733-9372(2005)131:8(1155)

Shokri-kuehni, S. M. S., Norouzi, M., Webb, C., Shokri, N., Zeiss, C., & Llc, M. (2017). Advances in Water Resources Impact of type of salt and ambient conditions on saline water evaporation from porous media, *105*, 154–161. https://doi.org/10.1016/j.advwatres.2017.05.004

Shuttleworth, W. J. (2012). *Terrestrial hydrometeorology*. Oxford,U.K: John Wiley & Sons.

Stull, R. B. (1988). *An Introduction to Boundary Layer Meteorology*. Dordrecht, Netherlands: Kluwer Academic.

Thompson, A. M., Kim, K., & Vandermuss, A. J. (2008). Thermal characteristics of stormwater runoff from asphalt and sod surfaces. *Journal of the American Water Resources*

Association, *44*(5), 1325–1336. https://doi.org/10.1111/j.1752-1688.2008.00226.x

Van Buren, M. A., Watt, W. E., Marsalek, J., & Anderson, B. C. (2000). Thermal enhancement of stormwater runoff by paved surfaces. *Water Research*, *34*(4), 1359–1371. https://doi.org/10.1016/S0043-1354(99)00244-4

Vercauteren, N., Huwald, H., Bou-Zeid, E., Selker, J. S., Lemmin, U., Parlange, M. B., & Lunati, I. (2011). Evolution of superficial lake water temperature profile under diurnal radiative forcing. *Water Resources Research*, *47*(9), 1–10. https://doi.org/10.1029/2011WR010529

Wang, Z., Bou-zeid, E., Smith, J. A., & Wang, Z. H. (2013). A coupled energy transport and hydrological model for urban canopies evaluated using a wireless sensor network 1644, (July), 1643–1657. https://doi.org/10.1002/qj.2032

Yoon, Y. N., & Wenzel, H. G. (1971). Mechanics of sheet flow under simulated rainfall. *Journal of the Hydraulics Division*.

Zhan, W., Ju, W., Hai, S., Ferguson, G., Quan, J., Tang, C., … Kong, F. (2014). Satellite-derived subsurface urban heat island. *Environmental Science and Technology*, *48*(20), 12134–12140. https://doi.org/10.1021/es5021185

Table 1. Input pavements thermal and hydraulic properties, source: (Pourshams-Manzouri, 2013)

Input	Pervious HMA	Impervious HMA	Pervious PCC	Impervious PCC	Symbol
Density (kg m^{-3})	2157	2238	2100	2100	ρ_g
Specific heat capacity (J kg^{-1} K^{-1})	900	900	950	950	c_g
Thermal conductivity (W m^{-1} K^{-1})	0.57	1.2	1.1	1.1	k_g
Streamwise length (m)	3.3	3.3	3.3	3.3	l
Porosity (non-zero for the pervious pavements)	0.21	-	0.21	-	φ

Figure Captions

Figure 1. (a): Important thermal processes in the heat budget of the problem illustrated for a rough surface, (b): Runoff and subsurface domains and their boundary conditions. The variables are as defined in section 2.1.2.

Figure 2. Experimental site and sensors. (a) the 4 types of pavements used (picture not from the present experiment: no stations were placed in the middle of each pavement), (b) the 3D printed hydrofoil with embedded thermocouples and the water depth sensor (CS616), (c) view of full set of instruments with the spray nozzles generating rain, and (d) the radiometer and WXT520 weather transmitter with a view of the runoff and rainfall impact.

Figure 3. Effect of the mixing factor β on the ground surface temperature (left), and runoff temperature at 2 mm above the ground (right)

Figure 4. Comparison of the roughness for the impervious and pervious pavements of the measurement field. HMA is Hot Mix Asphalt and PCC is Portland Cement Concrete (PCC).

Figure 5. Downstream runoff depth from the model output and the observations for impervious concrete (left), and impervious asphalt (right)

Figure 6. Ground surface temperature (top panel), runoff temperature at 2 mm above the ground (middle panel), difference between ground surface and runoff temperature at 2 mm (bottom panel) from the model and the observations for impervious concrete (left panel), and impervious asphalt (right panel).

Figure 7. Ground surface temperature from model output and the observations for pervious concrete (left), and pervious asphalt (right)

Figure 8. Left: averaged (along the pavement) ground surface, air (= rain) , and vertically-averaged effluent temperature time series (at downstream). Right: time evolution of the difference between ground surface and water surface temperature values for x = 1 m, x = 20 m, and x = 50 m.

Figure 9. Time series of the surface energy budget terms of the ground surface (left) and water surface (right) for the impervious (solid line) and pervious (dashed line) pavements.

Figure 10. Time series of different terms in the thermal budget of the whole water layer for the impervious parking pavement.

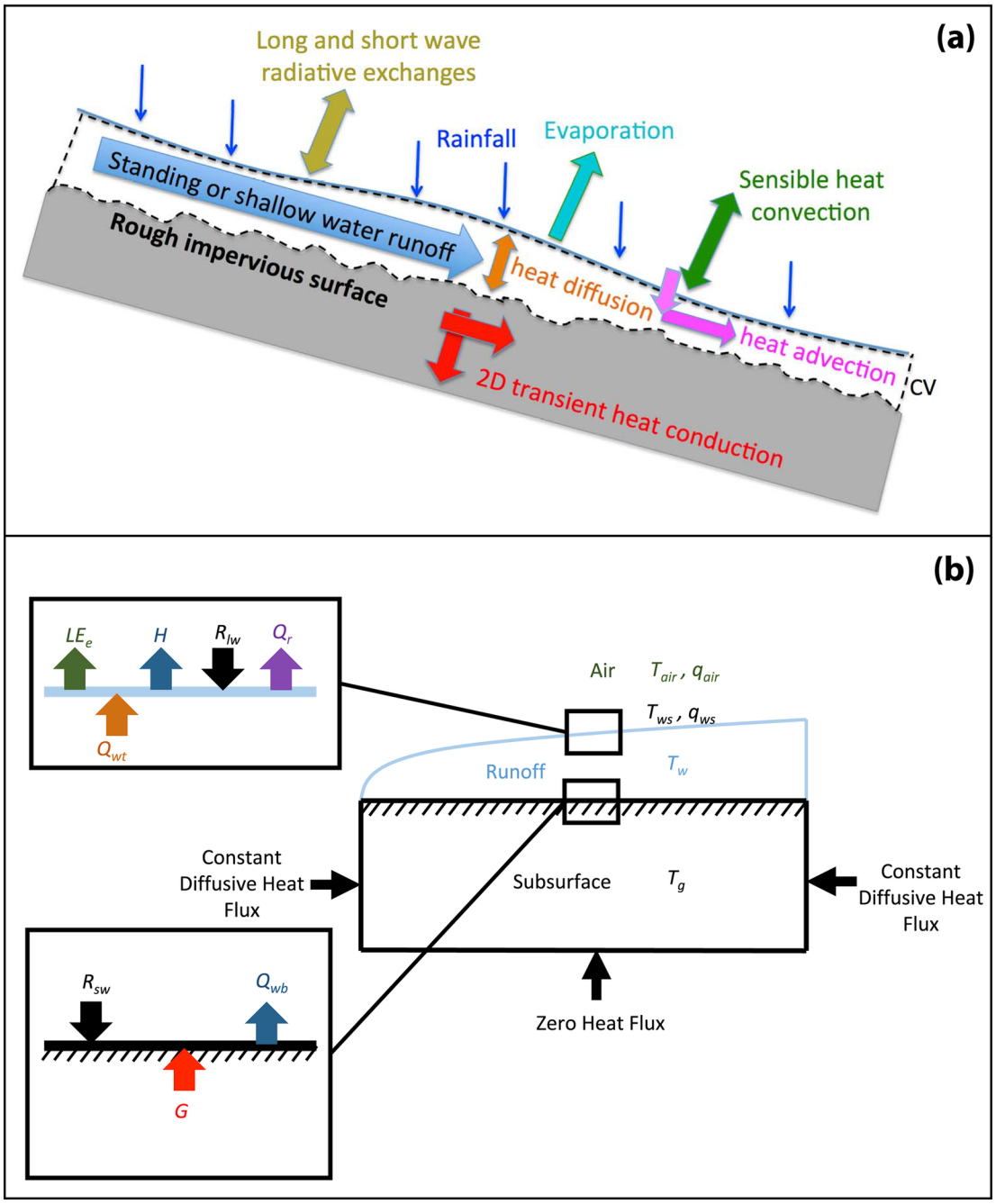

2017WR022241-f01-z-.tif

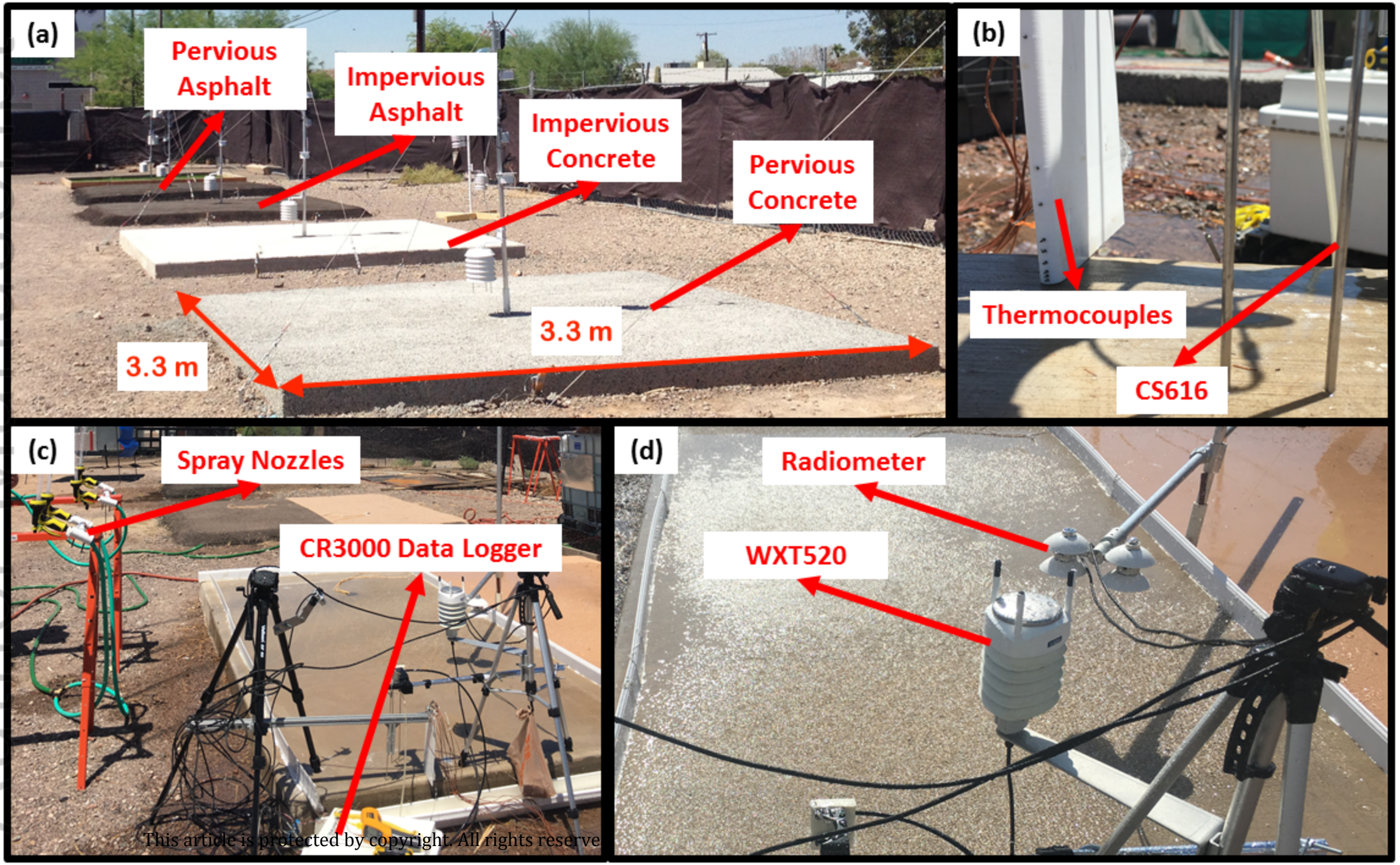

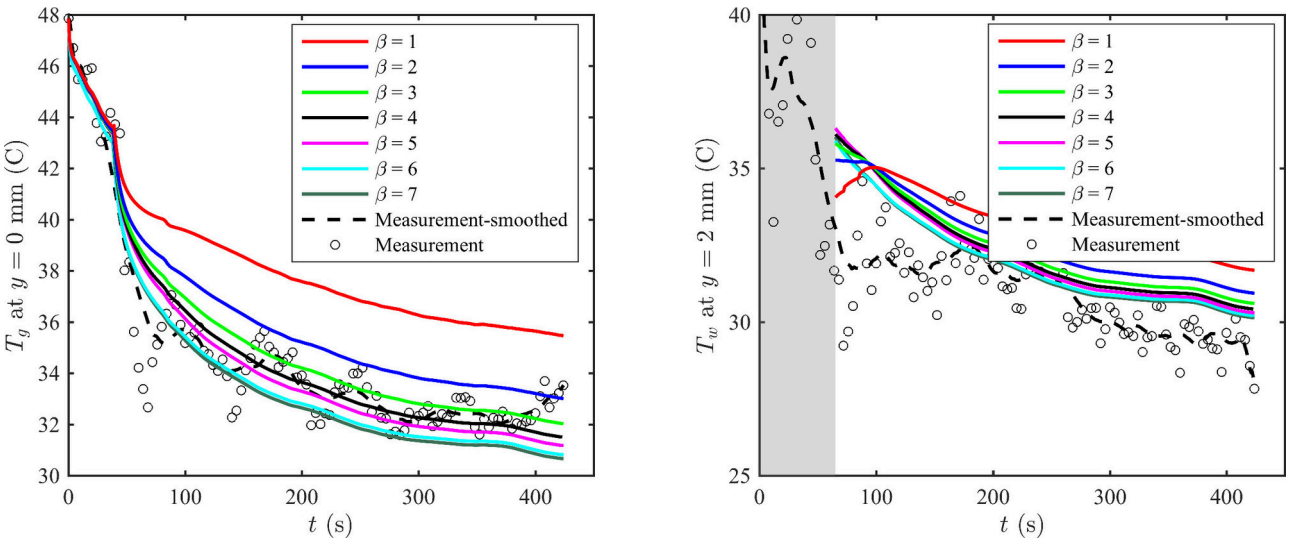

2017wr022241-f03-z-.eps

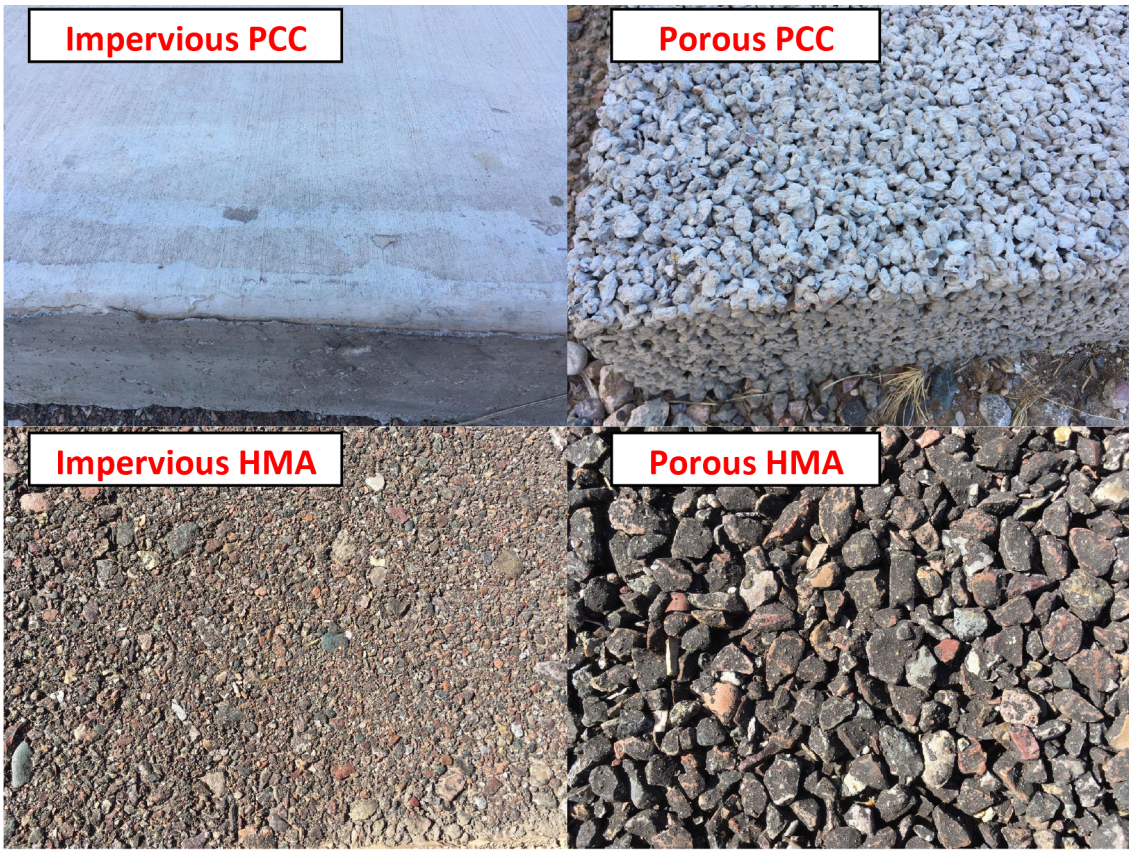

2017WR022241-f04-z-.tif

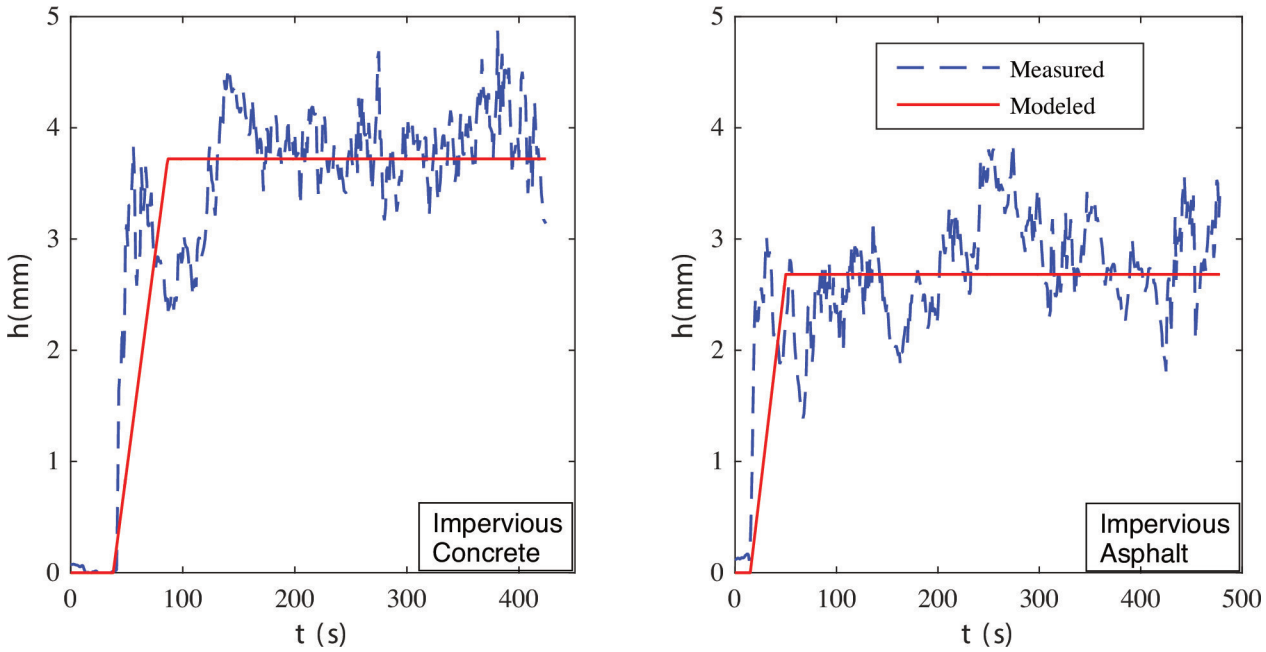

2017wr022241-f05-z-.eps

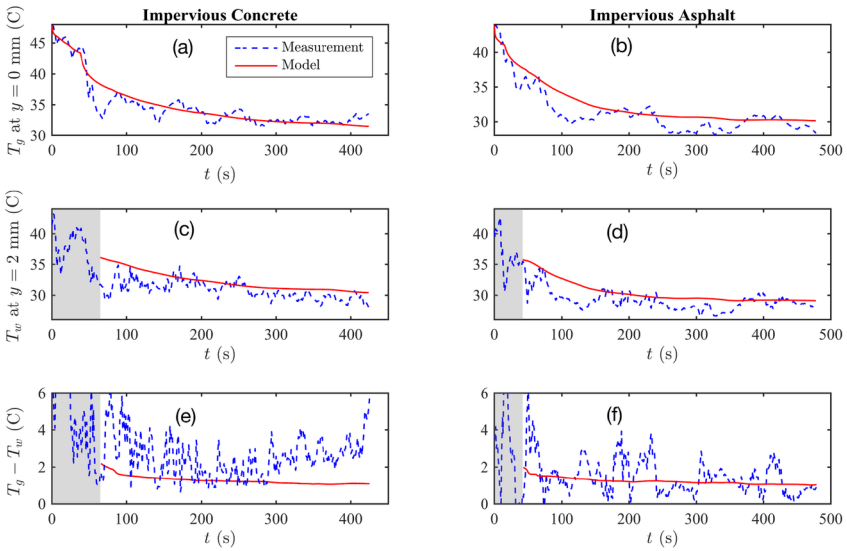

2017WR022241-f06-z-.tif

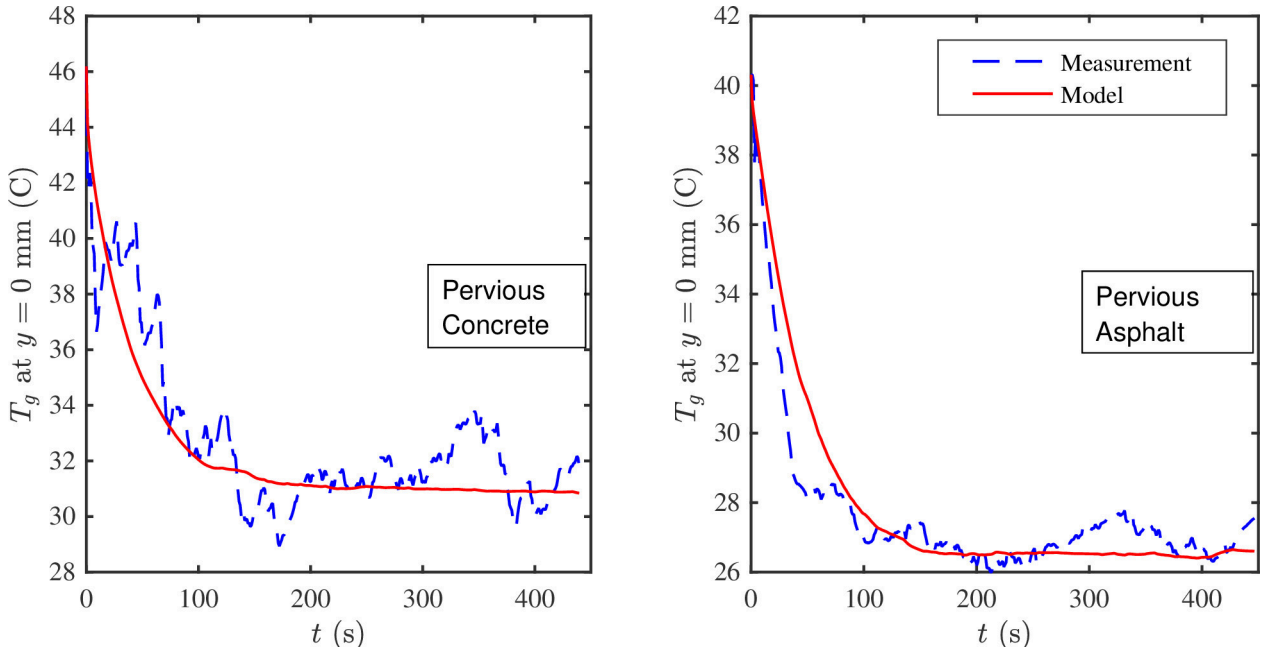

2017wr022241-f07-z-.eps

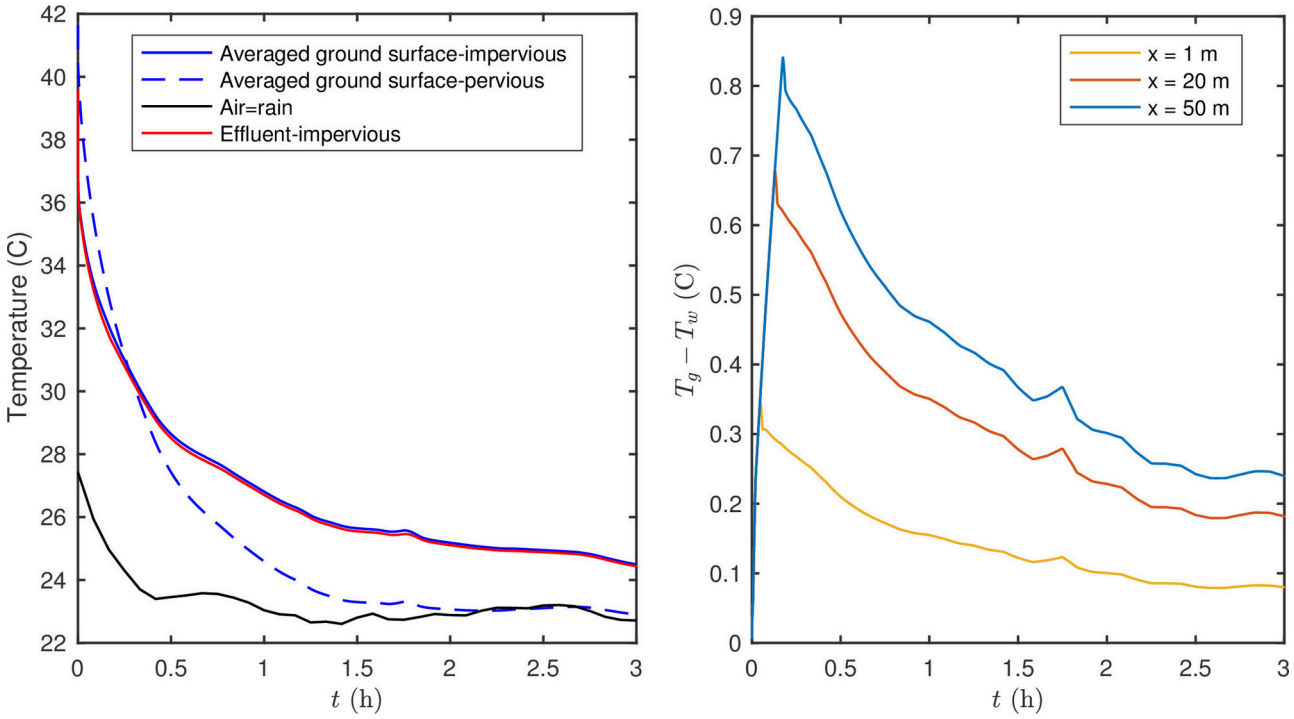

2017wr022241-f08-z-.eps

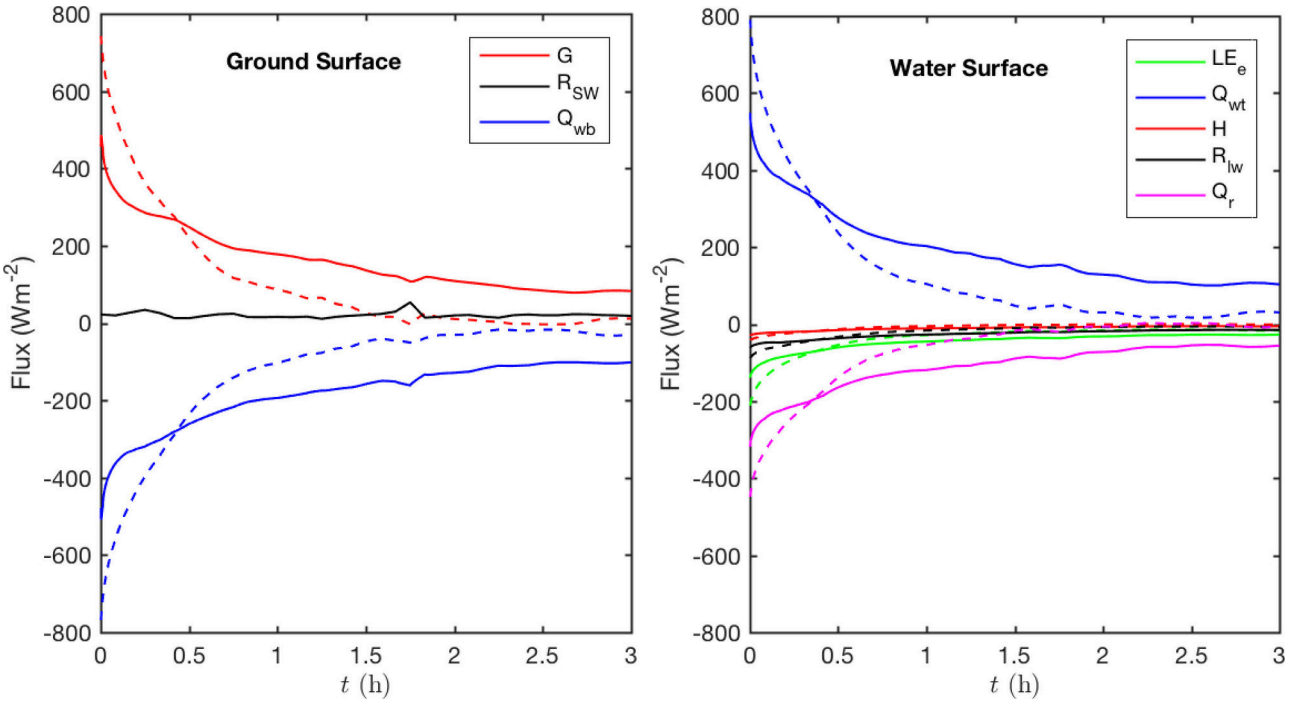

2017wr022241-f09-z-.eps

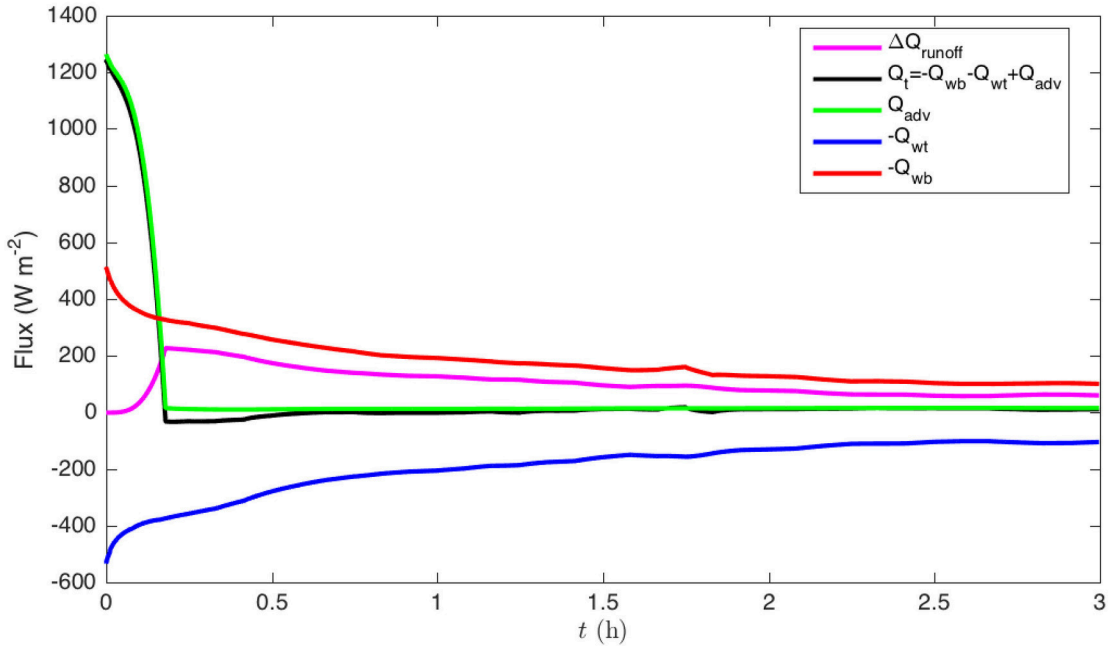

2017wr022241-f10-z-.eps